APPLIED
RESEARCH
LABORATORIES

ARL-TR-71-51
29 March 1972

SONAR ARRAY STUDIES
Final Report Under Contract N00014-70-A-0166
Task 0001, Item 9, Exhibit I

Jan M. Cooper, Louis H. Fowler

80

DOCUMENT CONTROL DATA · R & D

Security classification of title, body of abstract and indexing annotation must be entered when the overall report is classified

1. ORIGINATING ACTIVITY (Corporate author)	2a. REPORT SECURITY CLASSIFICATION
Applied Research Laboratories The University of Texas at Austin Austin, Texas 78712	UNCLASSIFIED
	2b. GROUP ---

3. REPORT TITLE

SONAR ARRAY STUDIES

4. DESCRIPTIVE NOTES (Type of report and inclusive dates)

final report   (1 December 1970 - 30 November 1971)

5. AUTHOR(S) (First name, middle initial, last name)

Jan M. Cooper, Louis H. Fowler, Frederick G. Anderson

6. REPORT DATE	7a. TOTAL NO. OF PAGES	7b. NO. OF REFS
29 March 1972	82	32

8a. CONTRACT OR GRANT NO.	9a. ORIGINATOR'S REPORT NUMBER(S)
N00014-70-A-0166 b. PROJECT NO. NR 240-014	ARL-TR-71-51
	9b. OTHER REPORT NO(S) (Any other numbers that may be assigned this report)
d.	

10. DISTRIBUTION STATEMENT

11. SUPPLEMENTARY NOTES	12. SPONSORING MILITARY ACTIVITY
Scientific Officer, Code 463, 202-692-4413	OFFICE OF NAVAL RESEARCH Department of the Navy Washington, D. C. 20360

13. ABSTRACT

This report summarizes work performed under Contract N00014-70-A-0166, Task 0001, Item 9, Exhibit I, Sonar Array Studies. The study described was aimed at developing design guidelines for sonar projecting arrays to be used for high source level, wide sector applications. The effort began with a literature survey described in the first two sections: "General Power Limits of Sonar Transducers," and Piezo-electric Properties of Ceramics." The piezoelectric equations of state are presented, along with a discussion of and results from two computer programs written to predict the performance of some different ceramics under various environmental and operational conditions. An analysis of beam patterns and directivity index of curved face arrays is presented in Section V. The final section contains conclusions and recommendations.

KEY WORDS	LINK A		LINK B		LINK C	
	ROLE	WT	ROLE	WT	ROLE	WT
projector						
ceramic						
curved face array						
source level						
directivity						
equivalent circuit						

DD FORM 1473 (BACK)
(PAGE 2)

ARL-TR-71-51
29 March 1972

SONAR ARRAY STUDIES
Final Report Under Contract N00014-70-A-0166
Task 0001, Item 9, Exhibit I

Jon M. Cooper, Louis H. Fowler

APPLIED RESEARCH LABORATORIES
THE UNIVERSITY OF TEXAS AT AUSTIN
AUSTIN, TEXAS 78712

ABSTRACT

This report summarizes work performed under Contract N00014-70-A-0166, Task 0001, Item 9, Exhibit I, Sonar Array Studies. The study described was aimed at developing design guidelines for sonar projecting arrays to be used for high source level, wide sector applications. The effort began with a literature survey described in the first two sections: "General Power Limits of Sonar Transducers," and "Piezoelectric Properties of Ceramics." The piezoelectric equations of state are presented, along with a discussion of and results from two computer programs written to predict the performance of some different ceramics under various environmental and operational conditions. An analysis of beam patterns and directivity index of curved face arrays is presented in Section V. The final section contains conclusions and recommendations.

TABLE OF CONTENTS

I. INTRODUCTION

This report summarizes the work performed under Contract
N00014-70-A-0166, Task 0001, Item 9, Exhibit I, Sonar Array Studies.
The purpose of this work was to investigate curved face array configu-
rations to provide guidelines for designing high acoustic power, high
search rate sonar transmitting arrays capable of large angular sector
coverage. High search rate sonars, operating at high power levels,
increase the probability of ceramic element failure resulting from
overheating and/or overstressing. Such instances have occurred with
some prototype and experimental projectors built at Applied Research
Laboratories (ARL). If, as proposed,[1,2] future generation transmitting
arrays are to be operated at even higher search rates and with an
order of magnitude increase over present operating power levels, it
seems imperative to know the effects of these future requirements on
sonar performance, so that adequate design guidelines may be formulated.
This report documents the results of a one year effort directed toward
prediction of projector performance.

To limit the problem to a manageable scope, the present effort
was concerned only with piezoelectric ceramic arrays. The dismissal of
magnetostrictive sources is at least partially justified in an effort
to obtain maximum acoustic output power:

> For low Q transducers, heavily loaded by radiation (low Q_m)
> the presently available nickel-cobalt alloys are capable of
> far less power/pound than are the lead zirconate titanate
> ceramics. On the other hand, the strength of the magneto-
> strictive metals is an important advantage, especially for
> large structures such as low frequency ring transducers ....
> Breakthroughs in fundamental research would probably be
> required, however, to put magnetostrictive materials in
> a position of general supremacy.[3]

1

Although hydroacoustic sources of sound are suited for low frequency applications,[4] the hydroacoustic projector was not considered since the primary interest in this study was the ultrasonic frequency range.

The study was conducted as parallel efforts in two areas: array configuration, and properties and limitations of the piezoelectric ceramic materials.

The remainder of this report is divided into five major sections. Section II deals with general power limitations of sonar transducers. Section III briefly reviews the important piezoelectric properties of ceramics and discusses some important factors which affect the various properties.

In Section IV, a theoretical analysis of transducer performance based on the piezoelectric equations of state is presented. A mathematical model is developed for a lossless, thickness-mode piezoelectric plate, and the equivalent circuit technique is demonstrated. The analysis is extended to include both mechanical and electrical losses in the ceramic. Details of two computer programs based on this analysis are discussed.

An analysis of curved face sonar arrays is given in Section V. Beamwidth and directivity index calculations are considered as a function of array configuration, element size and type, and amplitude shading techniques. A relationship between directivity, source level, and acoustic power is also given. The final section (VI) contains conclusions and recommendations.

2

II. GENERAL POWER LIMITS OF SONAR TRANSDUCERS

The power output of a sonar transducer may be considered to have an electrical, a mechanical, an acoustical, and a thermal limit. Woollett[5] discusses the electrical and mechanical limits for both an electric field transducer and a magnetic field transducer. The electrical limit is proportional to storable electric and elastic energies, mechanical Q, mechanoacoustical efficiency, and electromechanical coupling coefficient. Woollett's analysis was done for linear electroacoustic transducers. The limits on stored energy are imposed by such factors as insulation breakdown, depolarization of materials, distortion resulting from dielectric (and ferromagnetic) nonlinearities, and deterioration of efficiency resulting from a rise in the dissipation factor at high fields. Thus, it would seem that a dynamic approach to power limits would be required in considering the high power (and therefore high driving field) operating conditions. The mechanical limit depends on the transducer's capacity to store elastic energy and is primarily determined by the elasticity of ceramic or crystal transducers.

Urick[6] discusses the cavitation limitation of acoustic power. The expression relating cavitation threshold and sound pressure level is

$$I_c = \frac{\left[(0.707)\ 10^6\ P_c\right]^2}{\rho c} \times 10^{-7} = 0.3\ P_c^2\ W/cm^2 \quad ,$$

where

I_c = cavitation threshold, W/cm^2,
P_c = peak pressure of sound wave causing cavitation, atm,
ρ = density of water, g/cm^3,
c = sound speed in water, m/sec.

3

The cavitation limit for a given projector can be obtained by multiplying I_c by the surface area of the transducer and using P_c adjusted for operating depth. The cavitation threshold

$$I_c = 0.3 \, P_c^{\,2} \, A \quad ,$$

where A is the surface area of the projector (cm^2), represents the maximum working value for the power output (W) of the projector. At the limiting power level several phenomena begin to occur which degrade the projector performance. These include erosion of the projector surface, loss of acoustic power in absorption and scattering by the cavitation bubble cloud, a deterioration in the beam pattern of the projector, and a reduction of the acoustic impedance into which the projector must operate. The cavitation threshold is inversely proportional to pulselength and directly proportional to frequency. An approximation to measured values is shown in Dwg. AS-71-668.
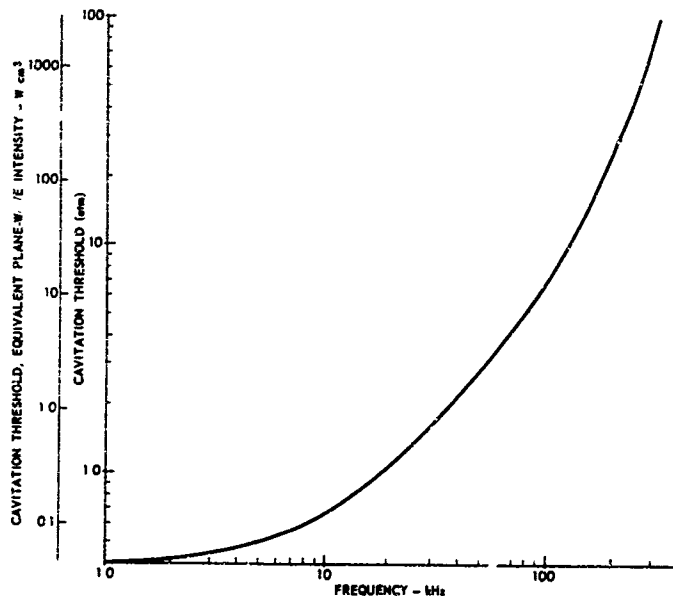
The sound pressure at the cavitation threshold is a function of depth (hydrostatic pressure),

$$P_c(h) = P_c(0) + \frac{h}{33} \, atm \quad ,$$

where h is in feet (33 ft of water is equivalent to 1 atm of pressure).

Sherman[7] introduced a factor γ to account for the nearfield effect on the cavitation threshold,

$$I_c = 0.3 \, \gamma \left(P_c(0) + \frac{h}{33} \right)^2 \quad .$$

CAVITATION THRESHOLD, EQUIVALENT PLANE W. /E INTENSITY – W cm²

CAVITATION THRESHOLD (atm)

FREQUENCY – kHz

A. FREQUENCY DEPENDENCE OF THE CAVITATION THRESHOLD
(cw Data on Fresh Water at Atmospheric Pressure)
(Adapted from Urick)[6]

CAVITATION THRESHOLD RELATIVE TO THRESHOLD AT 1 msec
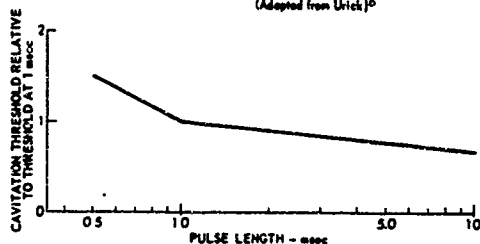
PULSE LENGTH – msec

B. AVERAGE VARIATION OF CAVITATION THRESHOLD WITH PULSE LENGTH
(Adapted from Urick)[6]

FREQUENCY AND PULSELENGTH DEPENDENCE
OF CAVITATION THRESHOLD

5

Experimental values for γ are between 0.3 and 0.6 for a circular piston, with an average of about 0.5. Therefore, the cavitation threshold of a transducer can be expressed as

$$I_c(f,h,\tau,A) = 0.15\left(P_c(0) + \frac{h}{33}\right)^2 \cdot g(f) \cdot e(\tau) \quad ,$$

where $g(f)$ is frequency dependence and $e(\tau)$ is the pulselength factor, as described in Dwg. AS-71-668.

The thermal limit of acoustic power is exceeded, for a transducer composed of piezoelectric ceramic, when the power dissipated within the element is sufficient to raise the temperature of the material to the Curie temperature. At the Curie temperature, the piezoelectric property is destroyed and is not restored when the ceramic cools.

The temperature behavior of a piece of piezoelectric ceramic is a function of time, of the thermal conductivity of the surrounding media, of ceramic volume, of ambient temperature signatures, and of the dissipation factor of the ceramic. The dissipation factor (tan δ) is the ratio of energy dissipated within the ceramic in the form of heat to the energy converted into mechanical motion. It varies with planar stress (hydrostatic pressure), driving field, and type of ceramic.

Only a limited amount of experimental or theoretical work has been published on the thermal behavior of electroacoustic projectors. Smith and Burbage[8] performed some experiments in connection with a comparative study of piezoelectric ceramics. They found that specimens of commercially available ceramics very similar in low field properties can show extreme variation in high field loss behavior. One anomaly observed at high operating fields was the occurrence of "hot spots," uneven heating of the ceramic.

6

III. PIEZOELECTRIC PROPERTIES OF CERAMICS

The power level capability of a projector is dependent upon properties of the piezoelectric ceramic. The values of these parameters are available from data sheets published by various suppliers. Typical values for piezoelectric ceramics commonly used in projectors are given in Table I.

Several studies of ceramic behavior under various operational and environmental conditions have been published in the literature. Drawings AS-71-669 through AS-71-674 are adaptations of experimental data. The ceramics are referred to by brand name, and only the behavior of projector materials is reported here.

Brown[9] tested the variations of several properties of PZT4 and NRE4 ceramics as a function of planar stress and electric field. Drawings AS-71-669, AS-71-670, and AS-71-671 are adaptations of his results, using one-dimensional static pressure for conventional mass loaded stacks. Martin[10] reported on the variation of coupling factor with pressure and his results are shown with Brown's in Dwg. AS-71-672.

Berlincourt[11] reported the behavior of dissipation factor as a function of electric field and temperature for the three Clevite projector materials, PZT4, PZT8, and Ceramic B. These results have been summarized in Dwg. AS-71-673.

Gerson[12] observed variations of mechanical Q and Young's Modulus as a function of stress (Dwg. AS-71-674). His work was done with two ceramic compositions with characteristics different from the so-called

7

TABLE I

SUMMARY OF PROJECTOR CERAMIC PROPERTIES

| Property (Symbol)	Definition	Principal Functional Dependence	Desired Features	Typical Value
Dielectric Dissipation Factor (tan δ_g)	Measure of the dielectric losses in the material—related to heat generated within the ceramic	Electric field strength; planar stress	Low	0.01 - 0.08
Curie Temperature	The temperature at which the crystal structure will permanently lose its piezoelectric activity	Electric field strength; time	High	300° - ~90°C
Electromechanical Coupling Constant (k_{ij})	A measure of the ceramic's ability to convert energy from one form to another. $k^2 = \dfrac{\text{mechanical output}}{\text{electrical input}}$	Ceramic's characteristic resonant frequency; strength of piezoelectric effect of ceramic	High	0.50 - 0.55
Planar coupling coefficient (k_p)	Combines the piezoelectric elastic and dielectric properties in a simple parameter	Natural mechanical resonance of ceramic	High	0.50 - 0.55
Strain constant (d_{ij})	An indication of piezoelectric sensitivity of ceramic. Relates mechanical strain to applied electric field. Measures the electric charge produced by a given force or the deflection produced by a given voltage across the material. $d = \dfrac{\text{strain developed}}{\text{applied field}}$	Electric force field applied	High	$d_{31} = -95 \times 10^{-12}$ $d_{33} = 220 \times 10^{-12}$ $\dfrac{C}{m}$
Voltage constant (g_{ij})	Relates open circuit voltage and mechanical stress. $g = \dfrac{\text{voltage}}{\text{stress}}$ $g = \dfrac{\text{open circuit field}}{\text{applied stress}}$	Stress applied	High	$g_{33} = 25 \times 10^{-3}$ $\dfrac{Vm}{N}$

8

TABLE I (Cont'd)

| Property (Symbol)	Definition	Principal Functional Dependence	Desired Features	Typical Value
Mechanical quality factor (Q_m)	Indicates the internal damping ability of a piezoelectric material. (Low Q_m indicates a high internal material damping ability.) Often the ratio of the energy stored over that lost in the energy dissipated in the load. (Ability to sustain ringing in hydrophone receptio.)	Resonant frequency	High	500
Dielectric constant (K)	Measure of the electric charge a piezoelectric shape can retain compared to the charge stored by equivalent electrodes separated by an air electrode. Ratio of $\dfrac{\text{permittivity of ceramic}}{\text{permittivity of free space}} = \dfrac{\varepsilon}{\varepsilon_o}$. where $\varepsilon_o = 9.0 \times 10^{-12}$ farad/meter. K directly affects the electrical impedance of the ceramic element.	Mechanical resonance of the ceramic. At resonance K is reduced by $(1 - k^2)$, where k is the coupling constant.	Low	1080 - 1300
Young's modulus (Y_{ij})	A measure of the elasticity of a ceramic; a ratio of the stress to the strain. (Ceramic is easier to deflect when sheared together by a wire.) $\dfrac{Y_{open}}{Y_{short}} \; \dfrac{(1 - k^2) = Y_{short}}{circuit}$ For $i = $ coupling coefficient. $k_{ij}^2 = d_{ij} \cdot g_{ij} \cdot Y_{ij}$	Ceramic's resonance frequency, stress level	High	$Y_{11} \cdot 11.0 \times 10^{10}$ $\dfrac{N}{m^2}$

9

TABLE I (Cont'd)

Property (Symbol)	Definition	Principal Functional Dependence	Desired Features	Typical Value
Elastic compliance (s_{ij})[19]	Measure of elasticity of ceramic $$s_{ij} = \frac{1}{Y_{ij}}$$ Is reciprocal of stiffness and is analogous to electrical capacitance	Ceramic's resonance frequency, stress level	Small	$\frac{m^2}{N}$

*Piezoelectric components are generally written as tensor components; k_{31} or k_{15}. These ij subscripts are related to orthogonal axes x, y, z represented as 1, 2, 3, respectively. The first subscript, i, is the electrical direction; the second, j, is the mechanical direction. The numbers 4, 5, 6 refer to shear in the yz, xz, and xy planes (around the x, y, and z axes), respectively; i.e., d_{31} is a measure of the deflection along the x-axis in response to a voltage applied parallel to the z-axis.[10]
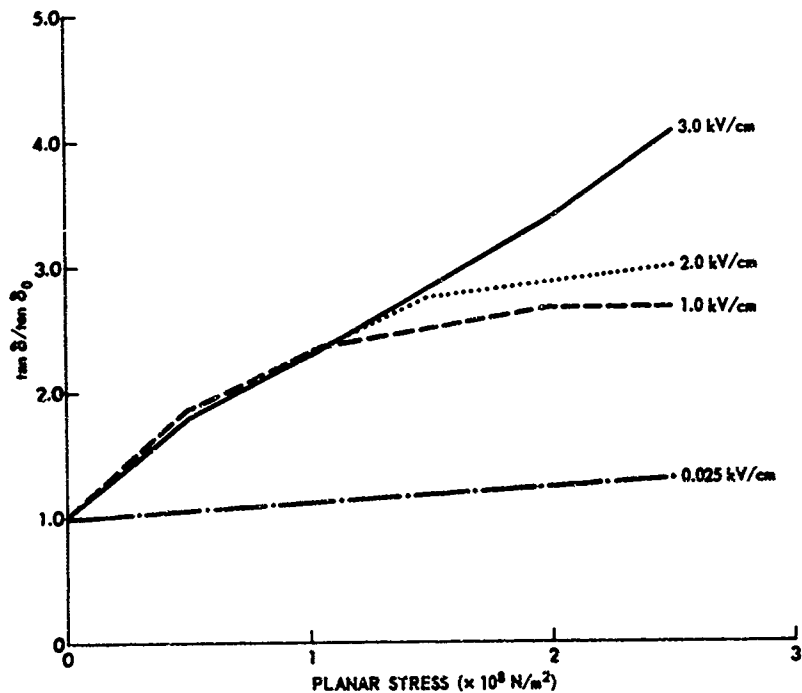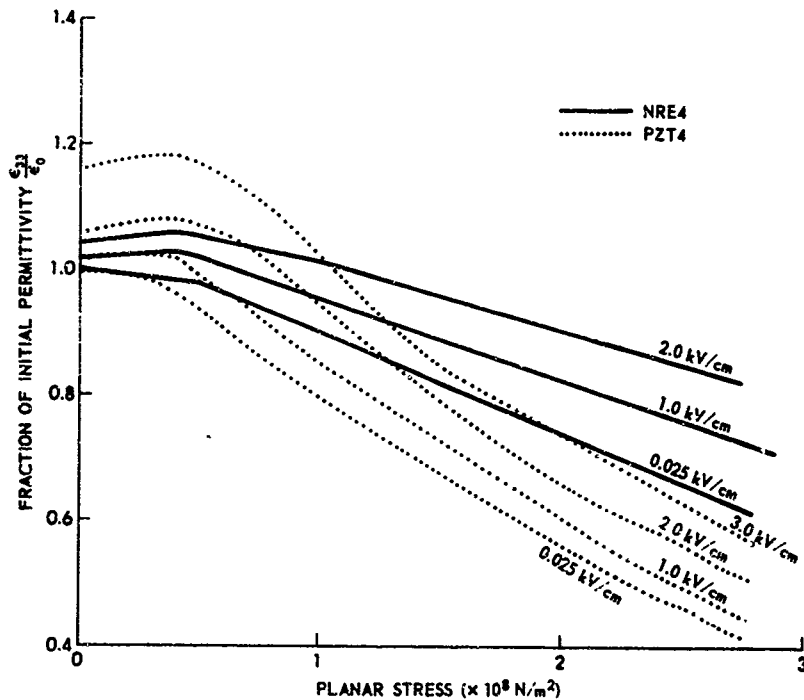

10
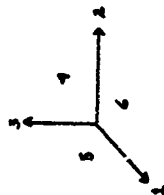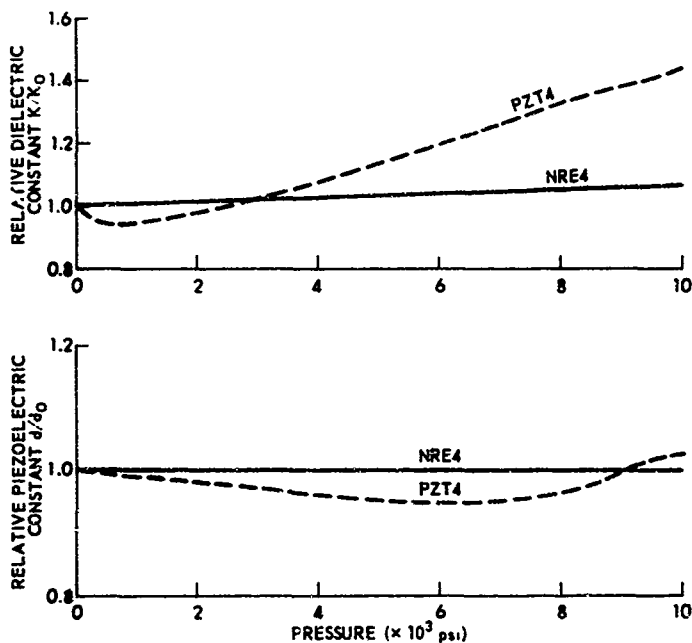
**VARIATION OF DIELECTRIC AND
PIEZOELECTRIC CONSTANTS WITH PRESSURE**
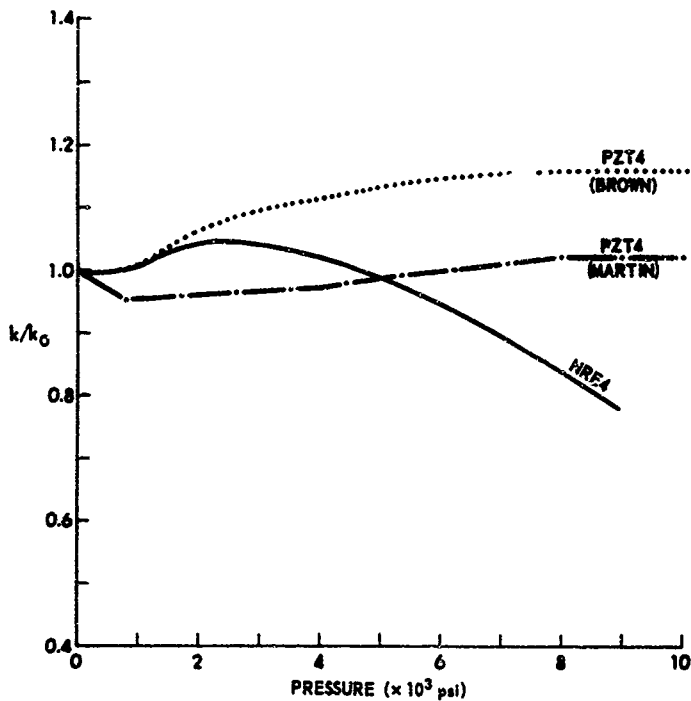(One-Dimensional Static Pressure for
Conventional Mass-Loaded Stacks)

VARIATION OF DISSIPATION FACTOR WITH
PLANAR STRESS AND ELECTRIC FIELD
(NRE4 and PZT4) (9)

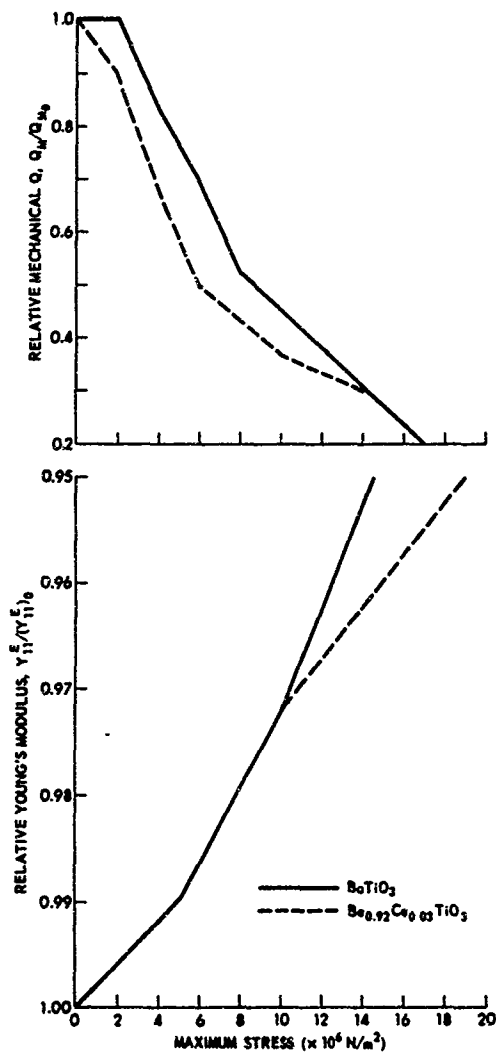**VARIATION OF PERMITTIVITY WITH PLANAR STRESS AND ELECTRIC FIELD FOR NRE4 AND PZT4 CERAMIC (9)**

VARIATION OF COUPLING FACTOR WITH PRESSURE FOR NRE4
AND PZT4 AS MEASURED BY BROWN (9) AND MARTIN (10)

14
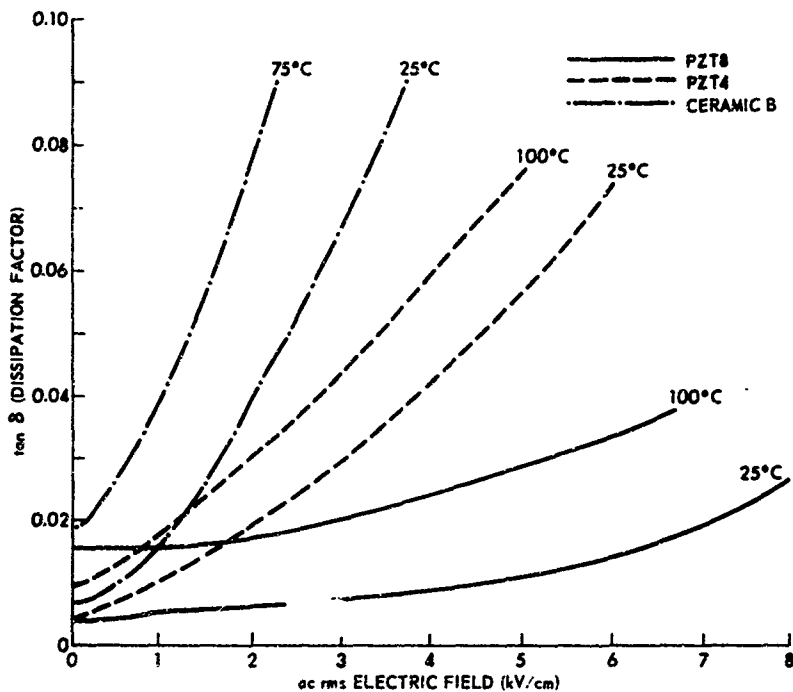
VARIATION OF DISSIPATION FACTOR WITH ELECTRIC FIELD
AND TEMPERATURE – PZT4, PZT8, AND CLEVITE CERAMIC B (11)

VARIATION OF MECHANICAL Q AND
YOUNG'S MODULUS WITH STRESS (12)

projector materials. No such data have been found on this particular
type of ceramic used in projectors. Gerson's results are reproduced
here only as an example of what may happen under certain conditions.

## IV. TRANSDUCER ANALYSIS BASED ON PIEZOELECTRIC EQUATIONS OF STATE

In this section, the piezoelectric equations of state will be used to develop a mathematical model of a thickness mode piezoelectric plate in which both electrical and mechanical losses are taken into account. Once the equations have been developed for the general case, an equivalent circuit will be developed for the idealized case of a thickness mode ceramic with no internal losses. Several examples are cited from the literature in which equivalent circuit techniques were used to obtain design guides for transducer performance (resonance frequency, power input, power output, dissipated power, impedance). In the remainder of this section, two computer programs written to predict transducer performance are discussed. The programs involve an exact solution to the piezoelectric equations developed at the beginning of this section. The first program, CERAMIC, predicts transducer performance as a function of frequency and drive level. The second program, CALTEMP, predicts the temperature rise and associated effects on ceramic performance resulting from the calculated power dissipated in the ceramic.

A. 3-Port Equations for Thickness Mode Piezoelectric Plate with Losses Included

A common mode for driving sonar projectors is that in which the applied electric field is parallel to the direction of elastic wave propagation, and the crystal is expanded in the thickness direction as shown in Dwg. AS-71-1101.

Preceding page blank

19
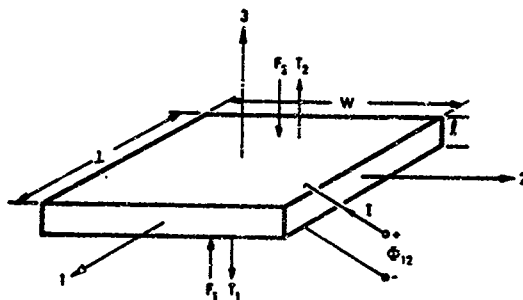
BROAD PLATE RESONATOR GEOMETRY

AS-71-1101

It is assumed (1) that the length and width dimensions are sufficiently large so that displacements occur only in the thickness direction, (2) that the two plane surfaces of area $l \times w$ are equipotential surfaces, and (3) that the magnitudes of applied or produced electrical or mechanical stresses are small enough to insure linear operation.

If mechanical losses proportional to the strain rate are assumed, then the equation for the generated stress may be written

$$T = c^D(1+j \tan \delta_c)S - hD \quad ,$$

where

c^D is the stiffness constant,

S is the strain,

h is a piezoelectric constant,

D is the electric displacement,

j is $\sqrt{-1}$, and

$\tan \delta_c$ is the mechanical "loss tangent" of the ceramic.

By definition, the loss tangent is the ratio of the elastic energy dissipated to the elastic energy stored per radian. For one-dimensional motion in the 3 direction, the stress equation is

$$T_3 = c^D_{33}(1+j \tan \delta_c)S_3 - h_{33}D_3 \quad .$$

The time-independent electric field equation of state is given by

$$E_3 = -h_{33}S_3 + \frac{1}{\epsilon^*_{33}} D_3$$

$$= -h_{33} \frac{\partial u(z)}{\partial z} + \frac{1}{\epsilon^*_{33}} D_3 \quad ,$$

where ϵ^*_{33} is the complex dielectric permittivity defined as

$$\epsilon^*_{33} = \epsilon^s_{33} \left(1 - j \tan \delta_E\right) \quad .$$

The quantity ϵ^s_{33} is the real permittivity measured at constant strain and $\tan \delta_E$ is the electrical loss tangent for the ceramic. The (peak) applied voltage is given by

$$\phi_{12} = -\int_{z=0}^{z=\ell} \vec{E} \cdot \vec{dz} \quad .$$

The face velocities and the input current obtained for the 3-port equations are (time dependence is suppressed):

$$V_2 = -\frac{\phi_{12} Z_{13}\left(Z_{12} - Z_{11}\right)}{Z_{33}\left(Z_{11} Z_{22} - Z_{12}^2\right) + Z_{13}^2\left(2Z_{12} - Z_{11} - Z_{22}\right)} \quad ,$$

$$V_1 = \frac{\phi_{12} Z_{13}\left(Z_{12} - Z_{22}\right)}{Z_{33}\left(Z_{11} Z_{22} - Z_{12}^2\right) + Z_{13}^2\left(2Z_{12} - A_{11} - Z_{22}\right)} \quad ,$$

$$I = \frac{\phi_{12}\left(Z_{11} Z_{22} - Z_{12}^2\right)}{Z_{33}\left(Z_{11} Z_{22} - Z_{12}^2\right) + Z_{13}^2\left(2Z_{12} - Z_{11} - Z_{22}\right)} \quad ,$$

with the impedance parameters Z_{ij} defined as follows:

$$Z_{11} = ZL1 - jZ_0 \cot \gamma\ell \quad ,$$

$$Z_{22} = ZL2 - jZ_0 \cot \gamma\ell \quad ,$$

$$Z_{12} = jZ_0 \csc \gamma\ell \quad ,$$

$$Z_{13} = -j \frac{h_{33}}{\omega} \quad ,$$

$$Z_{33} = -j \frac{1}{\omega \epsilon_{33}^* A} \quad .$$

Detailed derivations of these equations appear in contract status
reports for 1 December 1970 - 30 May 1971[14] and 1 June 1971 -
31 August 1971.[15]

The 3-port equations are, within the limits of the assumptions
made, an exact description of the kinetic energy, the potential energy,
and the motion in the mechanical vibrating system as a function of
frequency. Because most engineers are more familiar with electrical
systems than with mechanical systems, mechanical systems are often
analyzed in terms of an equivalent electrical circuit. An electrical
circuit is analogous to a mechanical system if the differential equation
of the circuit is the same type as the differential equation which
describes the mechanical system and if the two systems exhibit identical
energy characteristics at each frequency.

B. Equivalent Circuit of Ideal (Lossless) Piezoelectric Plate

To illustrate the application of equivalent circuit techniques
and the way in which such analyses can yield useful design information,
the equivalent circuit for a thickness mode plate with no losses is
developed. Also, some results obtained through equivalent circuit
analysis by various authors are reproduced in this section.

The equivalent electrical circuit is obtained by assuming that
voltage is analogous to force, current to velocity, mass to inductance,
capacitance to mechanical compliance, and resistance to mechanical
resistance (the so-called "impedance" or "classical" analogy). Under

these assumptions, the equivalent circuit for the lossless, thickness mode plate can be shown to be the circuit given in Dwg. AS-71-1248, where

$$C_o = \frac{A\epsilon_{33}^S}{l}$$

and

$\phi = h_{33}C_o$ is the ideal transformer voltage ratio (the impedance ratio is ϕ^2).
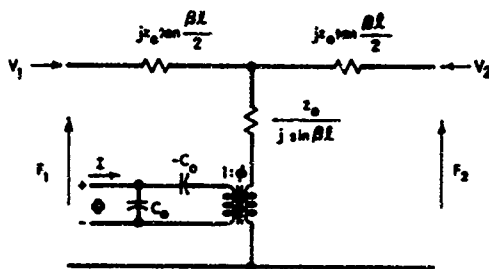
EXACT EQUIVALENT CIRCUIT FOR THICKNESS MODE PIEZOELECTRIC PLATE

ARL - UT
AS-71-1248
LFH - ORS
12 - 9 - 71

The circuit shown in Dwg. AS-71-1248 is an exact representation of the piezoelectric ceramic operating in the thickness mode and it is valid for any frequency. In using this circuit to describe a general situation in which the ceramic faces drive mechanical loads, it is necessary to connect to the mechanical terminals of the circuit the appropriate mechanical load impedances presented by the loads. The

final form for the distributed circuit with loads attached is shown in Dwg. AS-71-1025.
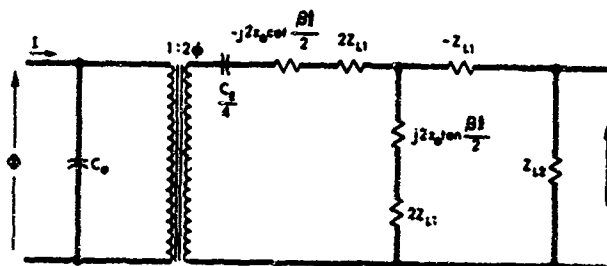
**FINAL FORM FOR DISTRIBUTED EQUIVALENT
CIRCUIT FOR THICKNESS MODE PIEZOELECTRIC PLATE**   AS-71-1025

If the resonator is operated near the mechanical resonance frequency $f_o \approx V_o/2l$, then the distributed impedances may be approximated by lumped impedances. It can be shown[16] that the term $j2Z_o \cot \beta l/2$ is approximated by a series-resonant circuit with a compliance C_m given by

$$C_m = \frac{1}{\pi^2 f_o Z_o}$$

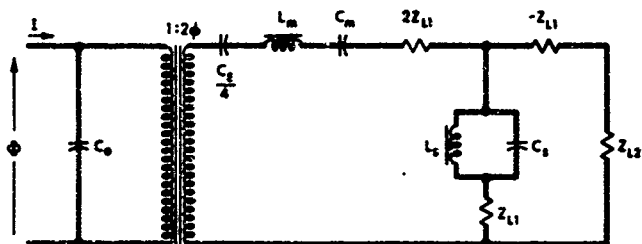and an inductance given by

$$L_m = \frac{1}{4\pi^2 f_o^2 C_m}\quad.$$

25

The $j2Z_o \tan \beta\ell/2$ is approximated by a shunt-resonant circuit for which

$$C_s = \frac{\pi^2}{18} C_m$$

and

$$L_s = \frac{1}{4\pi^2 f_o^2 C_s}$$

The equivalent circuit near resonance is shown in Dwg. AS-71-1026.

LUMPED ELEMENT EQUIVALENT CIRCUIT FOR
THICKNESS MODE PIEZOELECTRIC NEAR RESONANCE

AS-71-1026

C. <u>Optimum Design Considerations Based on Equivalent Circuits</u>

The application of electrical circuit theory as an aid in analyzing electro-mechano-acoustical vibrating systems has been well documented in the literature. The representation of a piezoelectric crystal as an equivalent electrical circuit element was originally given by Van Dyke.[16] The analysis of the piezoelectric transducer driving a mechanical and/or acoustical load has been discussed by Mason,[17,18] Olson,[19] and Katz,[20] as well as others. Work of a more

specific nature was conducted by Roth,[21] in which the equivalent circuit of a thickness mode piezoelectric transducer was used to determine the electrical driving point impedance as a function of loading and frequency. Thurston[22] has performed an analysis of the transducer loss and bandwidth as a function of mechanical and electrical loading based on the equivalent circuit for a piezoelectric transducer. Kossoff[23] has made use of equivalent circuit techniques in analyzing the effects of backing and matching on the performance of PZT7A transducer. Further references[24,25,26,27] of a more general nature are listed in the bibliography.

The effects of electrical and mechanical resistances on transducer loss and bandwidth have been analyzed by Thurston[22] for a transducer operating near resonance. Three cases are considered: (1) a transducer electrically tuned by a shunt coil, (2) a transducer tuned by a series coil, and (3) an untuned transducer. Some results of his analysis, given below, are valid for the case of a transducer free on one end or a transducer driving a symmetrical load on each end.

The transducer loss at resonance for a shunt-tuned transducer, as determined by Thurston, is shown in Dwg. A8-71-681 as a function of load and source resistance. Transducer loss is defined by
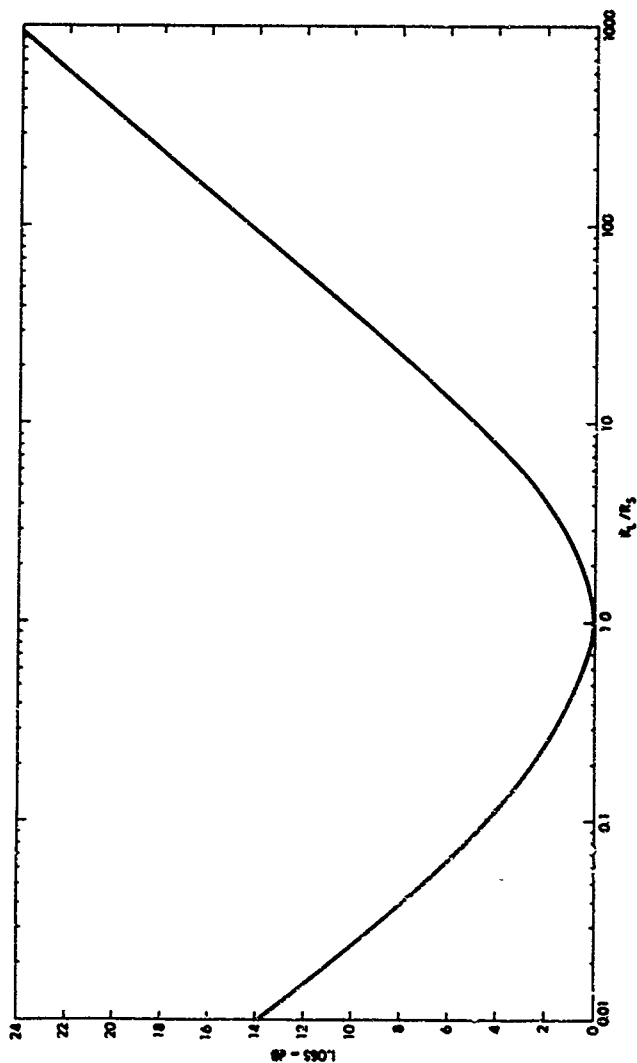
$$TL = 10 \log \frac{P_{max}}{P_a} \quad ,$$

where

P_a = power actually absorbed in load R_L,

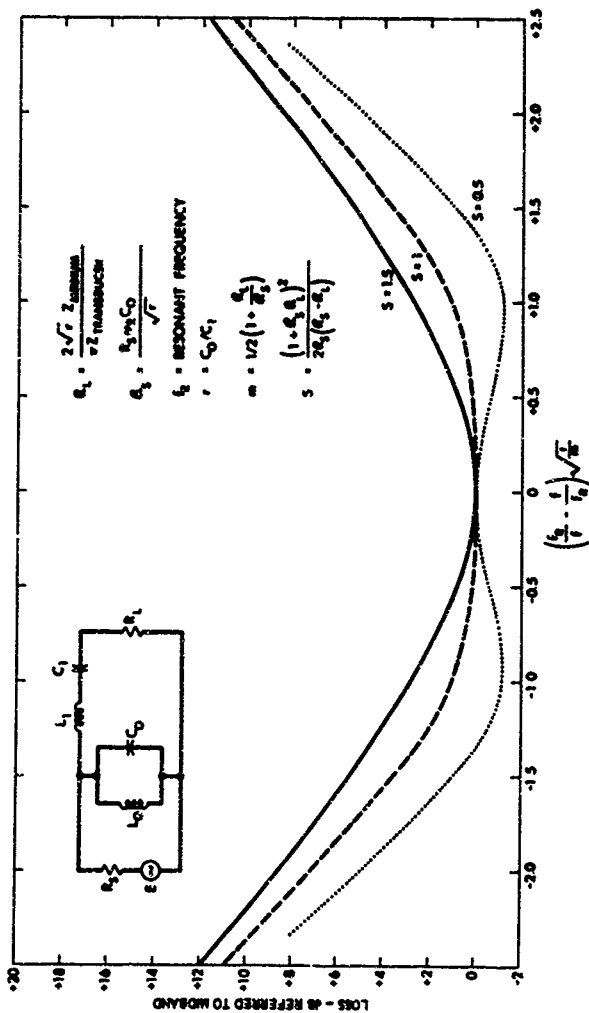P_{max} = power which would be absorbed if load and generator were matched.

The source impedance is the quantity R_s. The transducer loss as a function of frequency is shown in Dwg. A8-71-684.

TRANSDUCER LOSS AT
FREQUENCY OF RESONANCE (SHUNT COIL) (22)

ARL - UT
AS-71-681
LHF - RFO
3 - 21 - 71

28

TRANSDUCER LOSS AGAINST FREQUENCY (SHUNT COIL) (22)

For the case of the series-coil-tuned transducer, the results are essentially the same as the shunt-coil case, as long as the fractional bandwidth of the transducer is small. The fractional bandwidth (FBW) is given by

$$FBW = \frac{f_2 - f_1}{\sqrt{f_2 f_1}} \quad ,$$

where f_2 and f_1 are the high and the low cutoff frequencies respectively.

For the case of an untuned transducer, the transducer loss and the approximate FBW are given in Dwg. AS-71-683 as a function of the parameter α defined by

$$\alpha = \omega_R C_o R_L \quad .$$

The effects of backing and matching on the performance of piezoelectric transducers have been analyzed in a paper by Kossoff.[23] The analysis is valid for a thickness mode transducer for which the loading and backing media are large enough in extent so that no energy is reflected to the transducer. For the nonmatched cases, the transducer is assumed to drive directly into the loading and backing media.

Computer calculations were carried out by Kossoff for a PZT7A transducer, 2.5 cm diam, with a series-resonance frequency at 2 MHz. The transmitting sensitivity curves for several conditions of backing and matching are presented in Dwg. AS-71-682. The transducer is assumed to be driving into a water load. For those curves in which the transducer was matched either to the backing, the load, or both, the matching layer was assumed to be a quarter-wavelength thick at the transmitting resonance frequency,
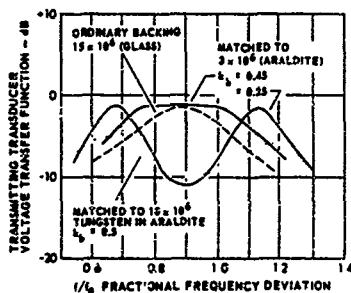
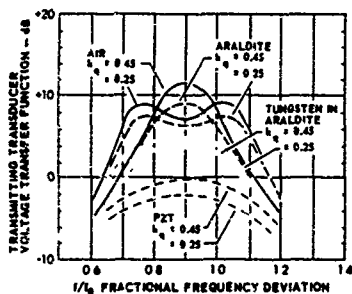$$f_o' = f_o \sqrt{1 - \frac{4 C_m}{|C_E|}} \quad .$$

30
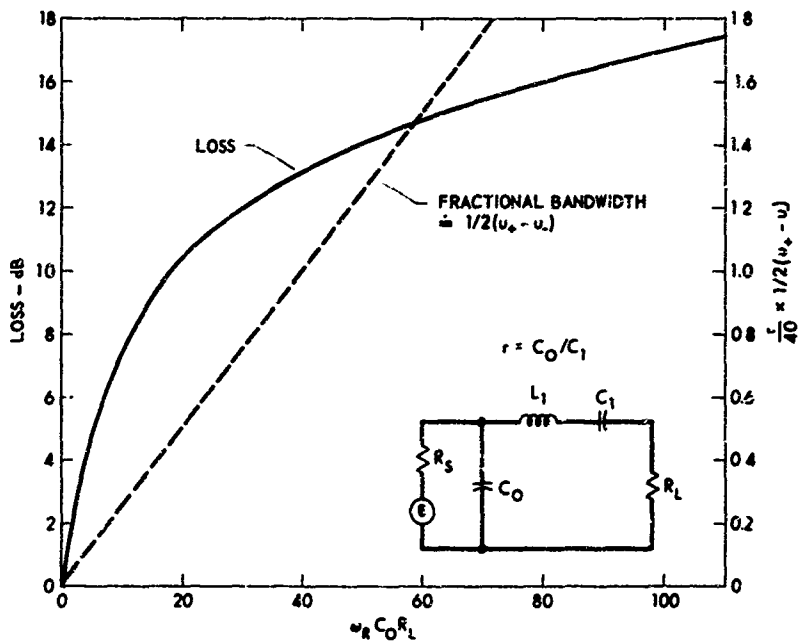
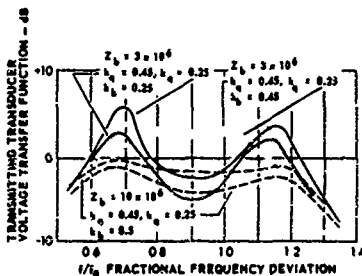BANDWIDTH AND LOSS WITHOUT A TUNING INDUCTOR (22)
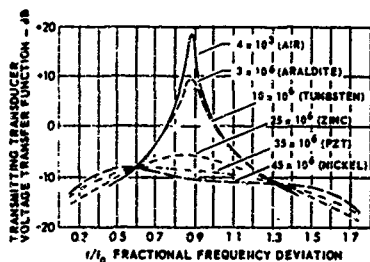
(a) BACKED TRANSMITTING TRANSDUCER
VOLTAGE TRANSFER FUNCTION

(b) MATCHED-TO-BACKING TRANSMITTING
TRANSDUCER VOLTAGE TRANSFER FUNCTION

(c) MATCHED-TO-LOAD TRANSMITTING TRANSDUCER
VOLTAGE TRANSFER FUNCTION WITH VARIOUS BACKINGS

(d) MATCHED-TO-LOAD MATCHED-TO-BACKING TRANSMITTING
TRANSDUCER VOLTAGE TRANSFER FUNCTION

EFFECTS OF BACKING AND MATCHING ON
TRANSDUCER PERFORMANCE [TAKEN FROM (23)]

(f_o is the series resonance of the L_m and the C_m circuit elements of Dwg. AS-71-1026 (see p. 26).)

The "z" and "k" quantities in the figures are defined by Kossoff as follows:

z_b = characteristic mechanical impedance of backing medium,

$k_b = z_b/z_{mb}$,

z_{mb} = characteristic mechanical impedance of quarter-wave section used to match transducer to backing medium,

z_q = characteristic mechanical impedance of loading medium

$k_q = z_q/z_{mq}$,

z_{mq} = characteristic mechanical impedance of quarter-wave load matching section.

From these analyses it is apparent that optimum power transfer occurs near the resonance frequency of the transducer with the load and source impedance matched. The bandwidth of the transducer is increased by matching either to the backing or to the load, but only at the expense of reduced output power. However, matching both to load and to backing produces a wide bandwidth as well as a satisfactory transmitting response.

D. Transducer Performance Predictions Based on Computer Solutions of 3-Port Equations

Two FORTRAN computer programs which were written to obtain theoretical performance data are discussed in this section.

1. Program CERAMIC

Program CERAMIC was written to obtain a solution to the 3-port equations as a function of frequency for the piezoelectric plate. The elastic, dielectric, and piezoelectric constants of the ceramic(s) (Section III) provide the necessary input data. The computer solutions

33

are obtained for ceramics operated at field levels for which input
data are available. The individual ceramic parameters must be specified
for each applied field level. In this study, three ceramics commonly
used and commercially available as projector materials, PZT8,
Channelite 5400, and Channelite 5800, were examined.

The complex expressions for the (time-independent) face velocities
and the input current are reprinted for convenience:

$$V_2 = -\frac{\phi_{12}z_{13}\left(z_{12}-z_{11}\right)}{z_{33}\left(z_{11}z_{22}-z_{12}^2\right) + z_{13}^2\left(2z_{12}-z_{11}-z_{22}\right)} \quad ,$$

$$V_1 = \frac{\phi_{12}z_{13}\left(z_{12}-z_{22}\right)}{z_{33}\left(z_{11}z_{22}-z_{12}^2\right) + z_{13}^2\left(2z_{12}-z_{11}-z_{22}\right)} \quad ,$$

$$I = -\frac{\phi_{12}\left(z_{11}z_{22}-z_{12}^2\right)}{z_{33}\left(z_{11}z_{22}-z_{12}^2\right) + z_{13}^2\left(2z_{12}-z_{11}-z_{22}\right)} \quad .$$

The equations for V_1, V_2, and I are solved by CERAMIC as functions of
frequency and field level and the values are used to calculate the rms
input and output powers and the rms dissipated electrical and mechanical
powers as functions and frequency for each field level. The rms
electrical input power for steady state current and voltage is given by

$$P = \frac{1}{2} \phi_{12} \left|I\right| \cos \theta \quad ,$$

where θ is the phase angle between ϕ_{12} and I. The input power per
volume of ceramic per kilohertz is given by

$$P = \frac{\phi_{12}^2 \, Re(Y_{1n})}{2A \cdot l \cdot f} \frac{W}{cm^3 \cdot kHz} \quad ,$$

where

$Re(Y_{in})$ is the total input conductance, and

Φ_{12} is expressed in volts, $A \cdot \ell$ in cubic meters, and f in kilohertz. The dielectric dissipated power (P_{DE}), determined from the rms loss current, is

$$P_{DE} = 10^7 \ \pi\epsilon_{33}^s \ \tan \delta_E \left(\frac{\Phi_{12}}{\ell}\right)^2 \ \frac{W}{cm^3 \cdot kHz} \quad ,$$

where (Φ_{12}/ℓ) is the electric field magnitude expressed in kV/cm.

The ceramic plate was arbitrarily assumed to have a radiating area of 0.01 m^2 and a thickness of 0.015 m. The values of the density and sound velocity for the acoustic medium (water) are, respectively, 10^3 kg/m^3 and 1500 m/sec. The remaining ceramic parameters necessary for the computer calculations are given in Table II. The velocity of sound in the ceramic was calculated from the given values of ρ and s_{33}^D,

$$v_o = \sqrt{\frac{c_{33}^D}{\rho}} \quad ,$$

based on the assumption that the stiffness constant is the inverse of the elastic compliance. The piezoelectric constant, h_{33}, is the product of the voltage constant and stiffness constant.

The input power, output power, and dissipated powers were calculated for each ceramic as a function of frequency for various drive levels. For PZT8, the applied electric field assumed integral values of 1, 2, ..., 7 kV/cm. The applied field values ranged from 1 to 4 kV/cm for Channelite 5400, and from 1 to 6 kV/cm for Channelite 5800.

35

TABLE II

CERAMIC PROPERTIES USED IN CALCULATIONS

Quantity	PZT8 [†]	Channelite 5400 [††]	Channelite 5800 [††]	Applied Field (kV/cm)(peak)
ρ(density), 10^3kg/m^3	7.6	7.6	7.6	-
Q_c, (1/tan δ_c)	1000	500	1050	-
g_{33}, 10^{-3}Vm/N	24.5	25.3	25.1	-
k_{33}	-	0.65	0.62	-
Y^E_{33}, 10^{10} N/m^2	-	6.75	7.30	-
s^D_{33}, 10^{-12} m^2/N	8.5	8.587 [†††]	8.434 [†††]	-
K^T_{33}	1000	1300	980	0
ΔK^T_{33}, %	0.2	1.0	0.3	1
	0.9	3.0	0.6	2
	1.4	6.0	1.1	3
	2.3	9.5	1.5	4
	3.0	-	2.0	5
	4.2	-	-	6
	6.0			7
tan δ_M	0.0048	0.009	0.00375	1
	0.006	0.015	0.004	2
	0.0069	0.02125	0.005	3
	0.0078	0.02765	0.006	4
	0.0088	-	0.00635	5
	0.010	-	0.00755	6
	0.0112		-	7

† Proc. IEEE 53, p. 1376.

†† Channel Industries Data Sheet.

††† Calculated from values of k_{33} and $Y^E_{33} = 1/s^E_{33}$; $s^D_{33} = s^E_{33}$ $(1-k^2_{33})$

As indicated in Table II, the values of the electrical loss tangent, tan δ_E, and the values of the electric permittivity were specified as a function of the applied field. The table lists the percent increase (from the no-field condition) in the relative dielectric constant, K_{33}^T, as a function of applied field. The permittivity at some field strength E at constant strain is calculated from $K_{33}^T(0)$, ΔK_{33}^T, and the coupling factor, k_{33}, by

$$\epsilon_{33}^s(E) = K_{33}^T \, \epsilon_0 \left(\frac{\Delta K^T}{100} + 1\right)\left(1 - k_{33}^2\right) \quad .$$

The reasonance frequency of a broad plate resonator is defined for the purposes of this report as the frequency of maximum input current. For thickness mode vibrating plate projectors that have a constant D $\cap$ boundary condition, it is pertinent to note that the reso...ance quency defined above does not occur at the frequency for which the plate thickness is equal to $\lambda/2$, where λ is the wavelength of the elastic disturbance in the ceramic. The deviation of the actual resonance frequency from the half-wave frequency is given by Kossoff[23] on the basis of equivalent circuit analysis,

$$f_0' = f_0 \sqrt{1 - \frac{4C_M}{|C_E|}} \quad ,$$

where C_M is the motional compliance of the near-resonance equivalent circuit and $\}$ is the negative compliance

$$C_E = -C_0/\varphi^2 \quad ,$$

where $\varphi = h_{33}C_0$ is the electromechanical transformer-turns ratio.

The capacitance C_0 is proportional to the permittivity, and the actual resonance frequency f_0' will be reduced as ϵ_{33}^s increases with

increasing field strength. This is illustrated in Dwg. AS-71-990, in which the ratio of the actual resonance frequency to the half-wave frequency, f_o'/f_o, is plotted as a function of applied field. These results were obtained from computer calculations for PZT8, Channelite 5400, and Channelite 5800. As can be seen from the graph, the reduction in resonance frequency is greatest for Channelite 5400 at all field levels.

The calculated dielectric loss power is shown as a function of applied field in Dwg. AS-71-991. The electric loss tangent was assumed constant with frequency and the results shown are independent of any frequency considerations. The mechanical power losses are plotted as a function of applied field in Dwg. AS-71-992. These plots were made from data calculated at the respective resonance frequency for each ceramic at each value of applied field strength and, therefore, represent the maximum loss as a function of applied field. The last set of curves shown in Dwg. AS-71-993 gives the calculated electro-acoustical efficiency η_{ea} as a function of applied field for each of the three ceramics. The plotted values correspond to the values of η_{ea} at the calculated resonance frequency of each respective ceramic at each value of applied field.

2.   Program CALTEMP

The results from program CERAMIC were obtained on the assumption that all of the energy dissipated in the ceramic was trans-mitted into the surroundings so that no change occurred in the ceramic temperature. To obtain a more realistic picture of transducer performance, it was essential to include a phenomenological description of a temperature rise in the ceramic resulting from the dissipated internal energy. This seemed especially necessary because future sonars will probably operate at higher search rates and at greater power levels than do present systems.

38
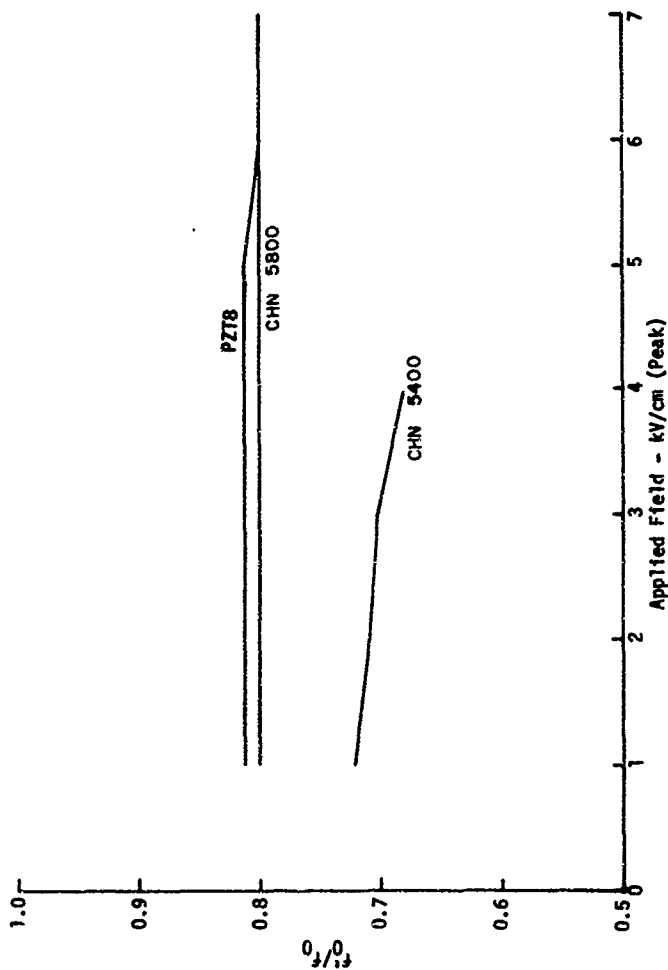
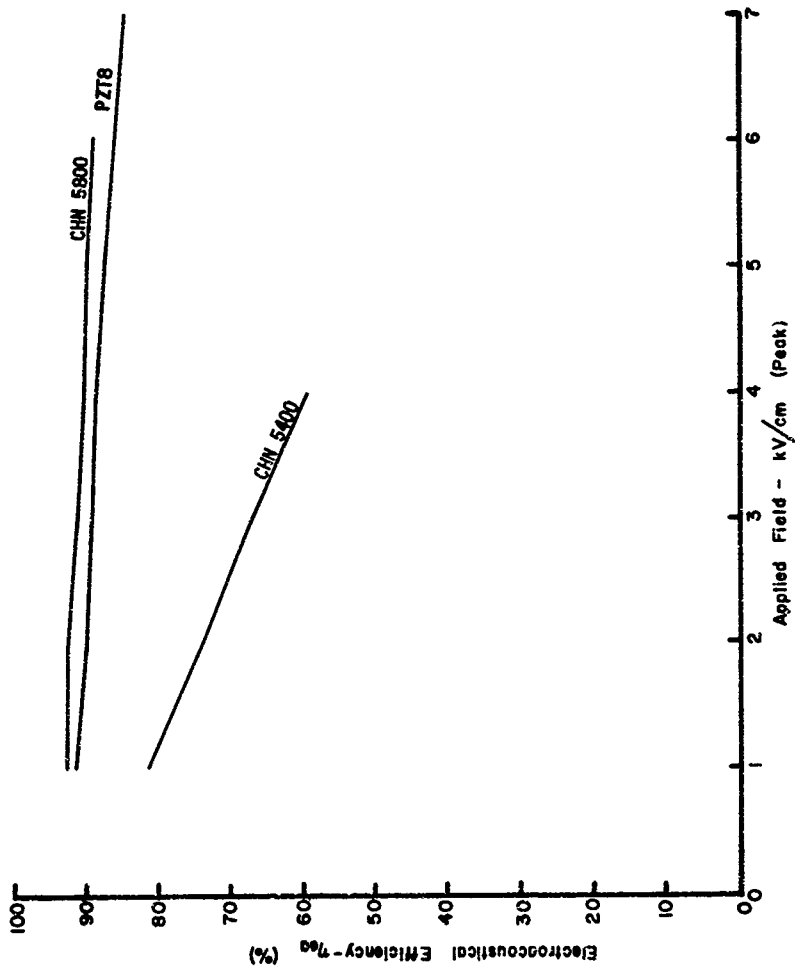REDUCTION OF RESONANCE FREQUENCY AS A FUNCTION OF APPLIED FIELD

AS-71-990

DIELECTRIC LOSS vs APPLIED FIELD
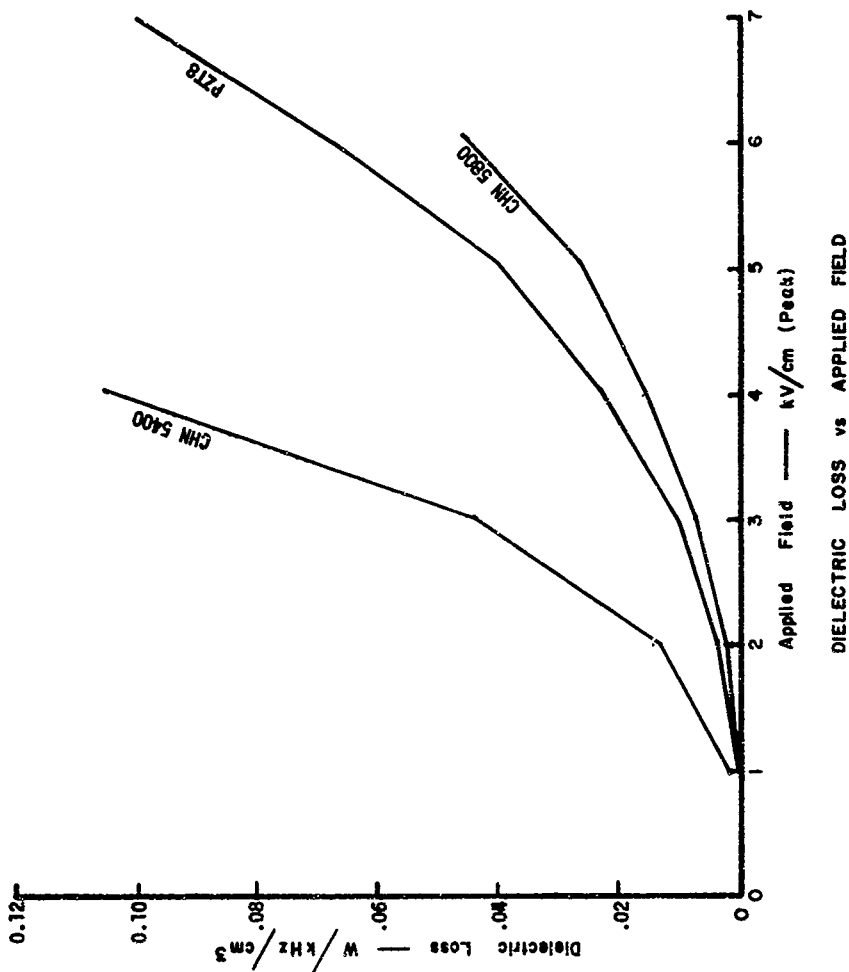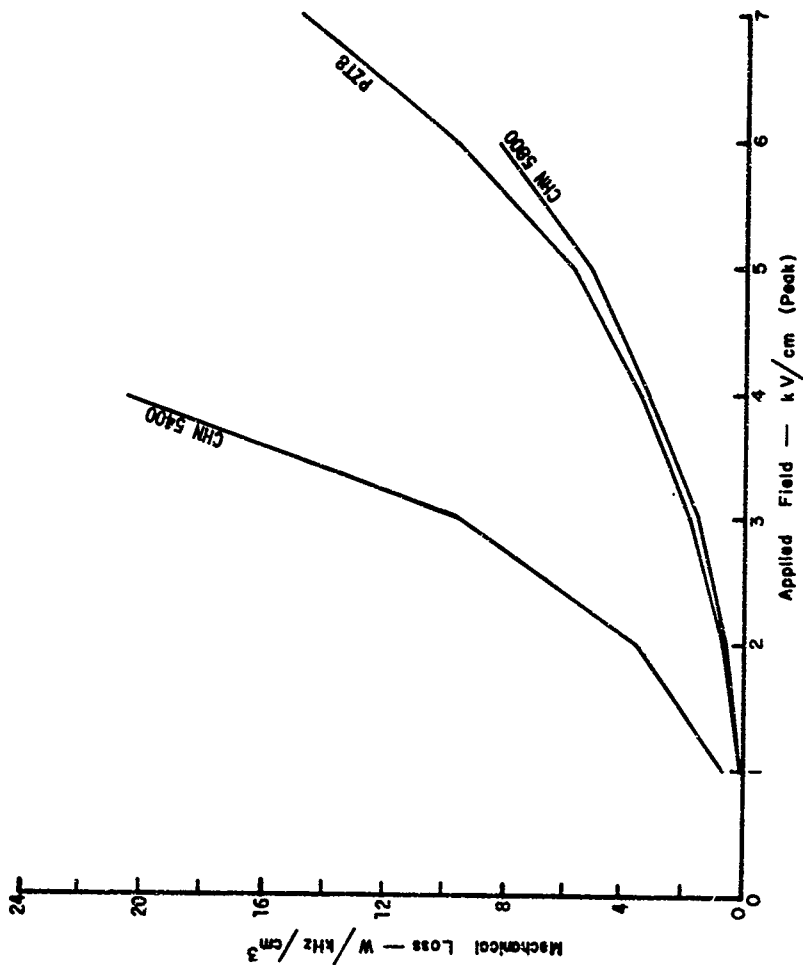
AS-71-991

MECHANICAL POWER LOSS AT RESONANCE AS A FUNCTION OF APPLIED FIELD

AS-71-992

41

ELECTROACOUSTICAL EFFICIENCY vs FIELD STRENGTH FOR PZT8, CHANNELITE 5400, AND CHANNELITE 5800

AS-71-993

Time was insufficient for detailed development of a temperature model; hence, what is presented here may appear somewhat oversimplified; however, this analysis is a beginning from which a more sophisticated description can evolve.

If Q represents the total power dissipated in the ceramic (in units of $W/cm^3/kHz$), then at a frequency f_o (kHz), the power/cm^3 dissipated in the ceramic is

$$PD = Qf_o (W/cm^3) \quad .$$

The dissipated power per kilogram of mass is then

$$1000 \ Qf_o/\rho \ (W/kg) \quad ,$$

where ρ is the density in g/cm^3. The specific heat, C_p, (J/kg/deg) can then be used to obtain the rate of temperature rise in the ceramic

$$\frac{\Delta T}{\Delta t} = 1000 \ \frac{Qf_o}{\rho C_p} \left(\frac{deg}{sec}\right) \quad .$$

To simplify the analysis, it is assumed that no heat transfer occurs from the ceramic to the surroundings. After a time τ the heat rise is

$$\Delta T = 1000 \ \frac{Qf_o}{\rho C_p} \ \tau$$

and

$$T_f = T_o + \Delta T \quad ,$$

where T_f and T_o are the final and initial temperatures, respectively.

43

The temperature model is completed by making the following assumptions:

1) the ceramic operates under steady state conditions during the time interval τ, and

2) no temperature change occurs during the period between the end of one time interval and the beginning of the next.

Because of these restrictions, the model can be interpreted as a cw system with a parameter update time τ or as a pulse mode system with a pulselength τ.

In program CALTEMP this temperature model was used to predict transducer performance, taking into account an associated ceramic temperature rise. The ceramic dimensions were assumed to be the same as in CERAMIC:

$$\text{Area} = 0.01 \text{ m}^2 \quad ,$$

$$\text{Thickness} = 0.015 \text{ m} \quad .$$

The load impedance on ceramic face 1 was assumed to be zero, and calculations were obtained for the case of an air load on face 2 as well as for the case of a water load.

The only ceramic for which parameter temperature data were available was PZT4.[24] The published data consist of the measured value of the dielectric constant at constant stress, K_{33}^T, and the electric dissipation factor, $\tan \delta_E$. Both parameters were measured at several temperatures for field levels of 1, 2, and 3 kV/cm. Using the published data, each parameter, at each field level, was estimated for each of 36 temperatures (the set $[T_s]$), and the results were read into the program as a 3×36 array for each parameter. A 1×36 array of the basic corresponding temperature set $[T_s]$ used in the calculation was also read in and will be referred to as the array T_s.

44

The relative dielectric constant at constant stress was converted to the value at constant strain from the relationship
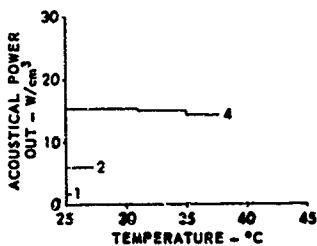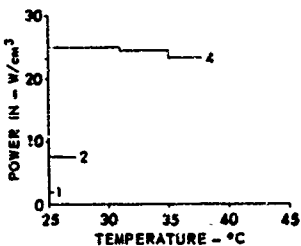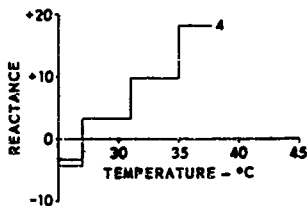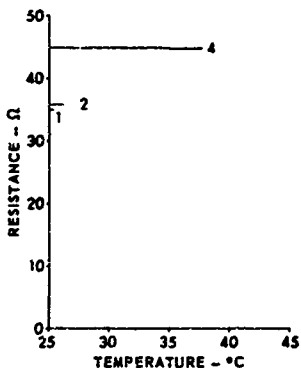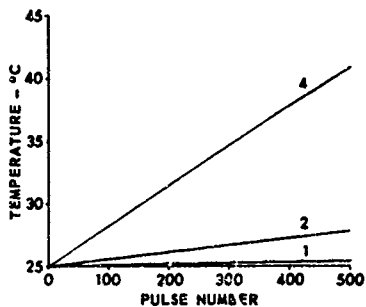
$$K_{33}^s = K_{33}^T \left(1-k_{33}^2\right) \quad ,$$

where k_{33} is the coupling factor. The initial ceramic temperature, T_o, was taken to be 25°C for each field level. The resonance frequency at that temperature was determined for each field level from program CERAMIC. These frequencies were used in CALTEMP as the operating frequency $f_o(L)$ for the appropriate field level L.

In CALTEMP, the expressions for V_1, V_2, and 1 are evaluated at the frequency $f_o(L)$ for each pulse and the input, output, and dissipated powers are calculated. The temperature T_f at the end of each pulse is determined and compared with the temperature values in the array T_s. The parameter values used for the next pulse are those corresponding to the temperature in the array T_s nearest the calculated ceramic temperature T_f.

The results obtained from CALTEMP for each sequence of 500 pulses (updates) are presented in Dwgs. AS-71-1315 through AS-71-1320. The first three sets of curves were obtained for bilateral radiation into a zero impedance load with pulselengths (parameter updates) of 100, 300, and 700 msec. The temperature versus pulse number, input resistance versus temperature, input conductance versus temperature, and input power versus temperature are plotted for each value of pulselength. A second set of similar graphs is shown for the case of air backing, with the ceramic radiating into a water load. In each set an additional curve is shown depicting the output power as a function of temperature.
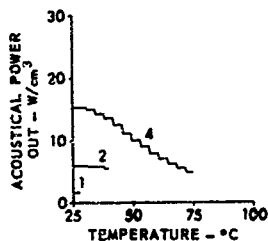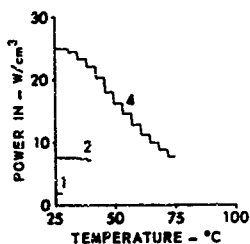
The temperature effects become more dramatic the longer the drive time and the greater the field strength. As indicated from

45

PERFORMANCE MEASURES FOR WATER LOAD, TAU = 100
FOR FIELD LEVELS OF 1, 2 AND 4-kV/cm

46

PERFORMANCE MEASURES FOR WATER LOAD, TAU = 300
FOR FIELD LEVELS OF 1, 2 AND 4–kV/cm

47
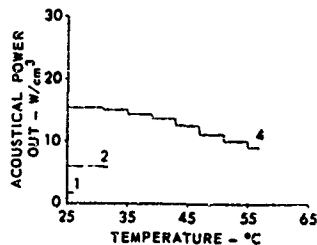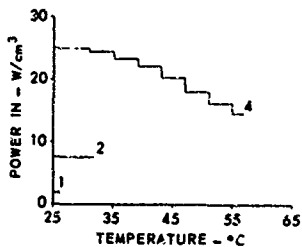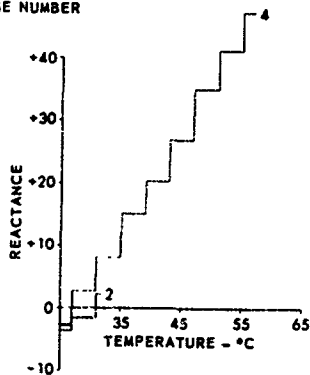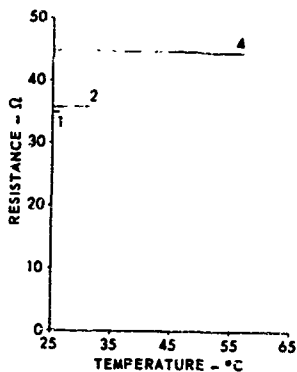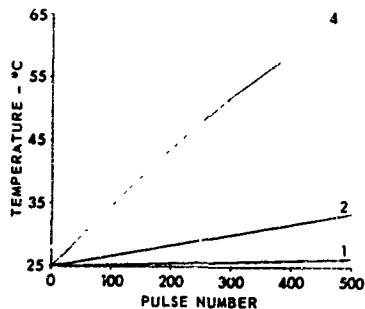
PERFORMANCE MEASURES FOR WATER LOAD, TAU ÷ 700
FOR FIELD LEVELS OF 1, 2 AND 4–kV/cm

PERFORMANCE MEASURES FOR AIR LOAD, TAU = 100
FOR FIELD LEVELS OF 1, 2 AND 4-kV/cm

49

PERFORMANCE MEASURES FOR AIR LOAD, TAU = 300
FOR FIELD LEVELS CF 1, 2 AND 4-kV/cm

50

PERFORMANCE MEASURES FOR AIR LOAD, TAU = 700
FOR FIELD LEVELS OF 1, 2 AND 4-kV/cm

51
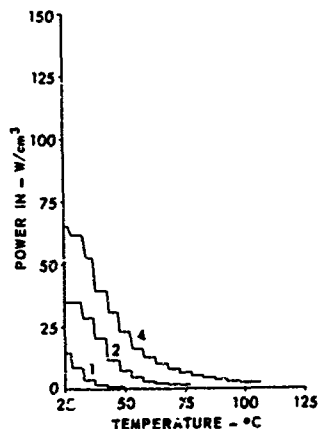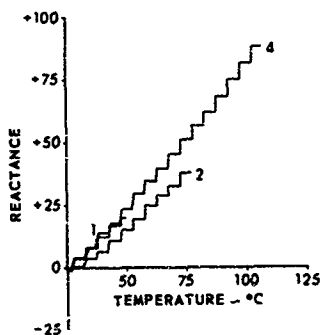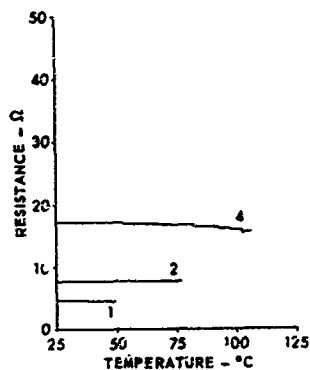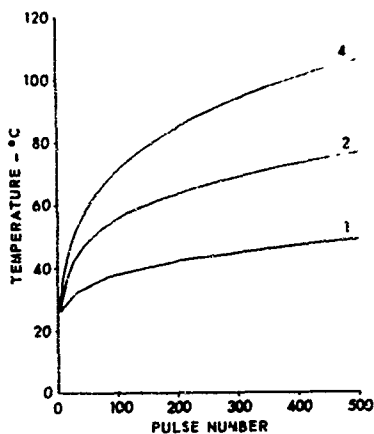
the resistance versus temperature curves, there is a reduction in the
input resistance as the temperature increases. The increase in
reactance with temperature indicates a shift in resonance to a lower
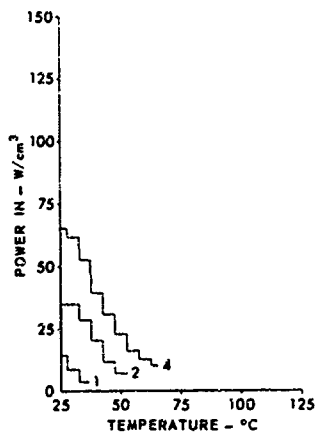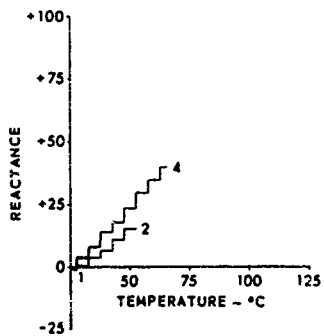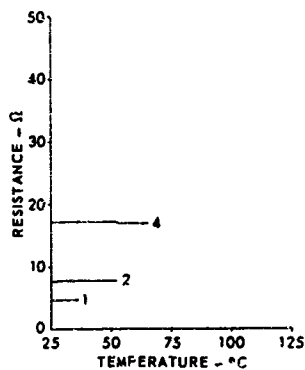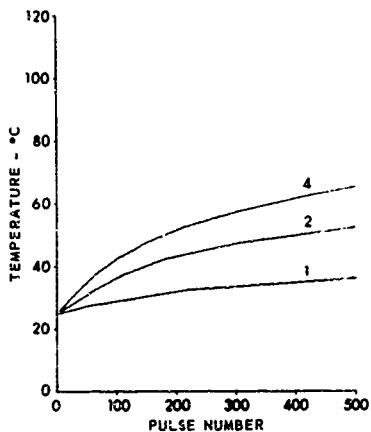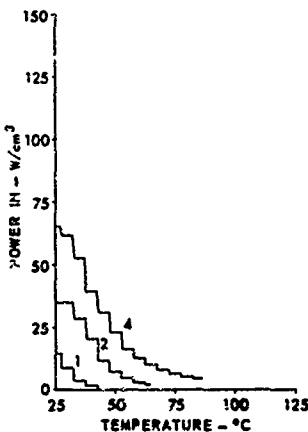frequency as the temperature increases. The severity of these effects
on the input power level is seen from the reduction of input power
as the ceramic temperature rises.

Experimental results of a similar nature have been obtained
by Kendig and Clarke.[28] They report a reduction of resonance frequency
with increasing temperature and an increase in input resistance with
increasing field strength. These results are consistent with those
presented here.

However, Kendig and Clarke also measured an increase in
input resistance with increasing temperature whereas CALTEMP calcula-
tions would indicate just the opposite. In their measurements, Kendig
and Clarke adjusted their operating frequency with temperature so that
their ceramic element was driven at resonance for all measurements.
In CALTEMP, the driving frequency was maintained constant at all tempera-
tures. No valid comparison of the results for resistance versus
temperature can, therefore, be made.

V. CURVED FACE SONAR ARRAY ANALYSIS

This section will cover the beam patterns of various curved face
arrays, directivity index of arrays, and source level, as related to
the array configuration.

A. Wide Sectors

Any beamwidth can be achieved with a planar array if power levels
inversely proportional to array length (and, therefore, amount of
ceramic in the projector) are acceptable. One technique for increasing
the amount of ceramic in a transducer without reducing the beamwidth is
to use a curved face array configuration. This can be done by either
using a section of a piezoelectric ceramic cylinder or by arranging
thickness mode staves vertically as though on the surface of a cylinder.
The former is the limiting case of the latter. As the staves become
more densely packed, the farfield beam pattern calculations become the
same.

The farfield pressure beam pattern of any array of discrete
radiators can be expressed as

$$P(\theta) = \frac{1}{N} \left| \sum_{k=1}^{N} E(\theta,k) \cdot A_k \cdot e^{i\psi(\theta,k)} \right| \quad ,$$

where

$E(\theta,k)$ is the response of the kth element in the θ direction,

A_k is the relative amplitude of the kth element and is proportional to driving voltage, mode coupling coefficient, and ceramic area of the kth element,

$\psi(\theta,k)$ is the phase of the contribution from the kth element in the θ direction. This may be due to electronic phasing and/or geometry of the array.

For the curved face array of identical, discrete, equally spaced line sources driven in phase, the contribution of the kth element in the θ direction is

$$E(\theta,k) = \frac{\sin\left(\frac{\pi s}{\lambda} \sin \gamma_k\right)}{\frac{\pi s}{\lambda} \sin \gamma_k} \quad ,$$

where

s is the length of each element, in inches,

λ is the wavelength, in inches,

and

$$\gamma_k = \theta - \left(\frac{N+1}{2} - k\right)\alpha \quad k = 1, 2, \ldots, n,$$

$$= \theta - \frac{\phi}{2} + (k-1)\alpha \quad ,$$

with

N = the number of radiators in the array,

α = angular spacing between element centers $\left(2 \cdot \sin^{-1}\frac{d}{2R} \text{ as shown in Dwg. AS-72-483}\right)$,

ϕ = angular width of the array (see Dwg. AS-72-483).

Each element is driven in exactly the same manner so that

$A_k = 1, k = 1, 2, \ldots, N \quad .$

54
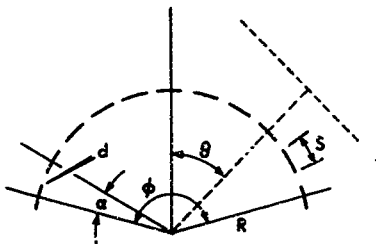
For an array of identical elements driven electrically in parallel under the same coupling mode conditions, the function ψ is given by

$$\psi(\theta,k) = \frac{2\pi R}{\lambda} \cos \gamma_k \quad ,$$

where

$\quad$ λ and γ_k are as defined above, and

$\quad$ R is the radius of curvature of the array, in inches.

There are several parameters which affect the behavior of $P(\theta)$. In order to isolate the effects of some of them, the following simplifications were made:

(1) To eliminate the frequency (wavelength) dependence, the distance measures are expressed in units of wavelengths:

$$s = \frac{s}{\lambda} \quad ,$$

$$R' = \frac{R}{\lambda} \quad , \text{ and}$$

$$d' = \frac{d}{\lambda} \quad .$$

55

(2) If the element size is allowed to approach zero, the $\frac{\sin x}{x}$ term in the summation is almost constant. In the limiting case,

$$\lim_{s' \to 0} \frac{\sin(\pi s' \sin \gamma_k)}{\pi s' \sin \gamma_k} = \lim_{s' \to 0} \frac{\left[\pi \sin \gamma_k [\cos(\pi s' \sin \gamma_k)]\right]}{\pi \sin \gamma_k} = 1$$

for all γ_k.

In the past, curved face projectors built at ARL have been required to insonify a maximum sector of about 70°. As a general rule, ARL curved face projectors have been constructed with an arc of angular width approximately 15% to 20% larger than the desired beamwidth; for example, to achieve a 60° beamwidth, an arc of approximately 70° was used. This general rule is also valid for wider beamwidths. A series of patterns was calculated for different angular width arrays and radii of curvature of 5λ, 10λ, 20λ, and 50λ. The elements were assumed omnidirectional to eliminate the effect of the individual element patterns in the calculation. The relationship between the array parameters R and Φ and the beamwidth is shown in Dwg. AS-71-701.

With linear arrays, a zonal shading technique will broaden the beam as well as lower the side lobe levels, so that a wider sector can be covered without much loss in directivity index. Patterns utilizing several zonal schemes with curved face arrays were calculated. Four patterns are shown in Dwg. AS-71-1086 which illustrate the effects of shading. All patterns are for an array of 65 point sources, equally spaced around a 130° arc with radius of curvature of 10 wavelengths. The directivity is increased by these zonal shading techniques, but this increase is due to a severe narrowing of the main beam rather than side lobe suppression.
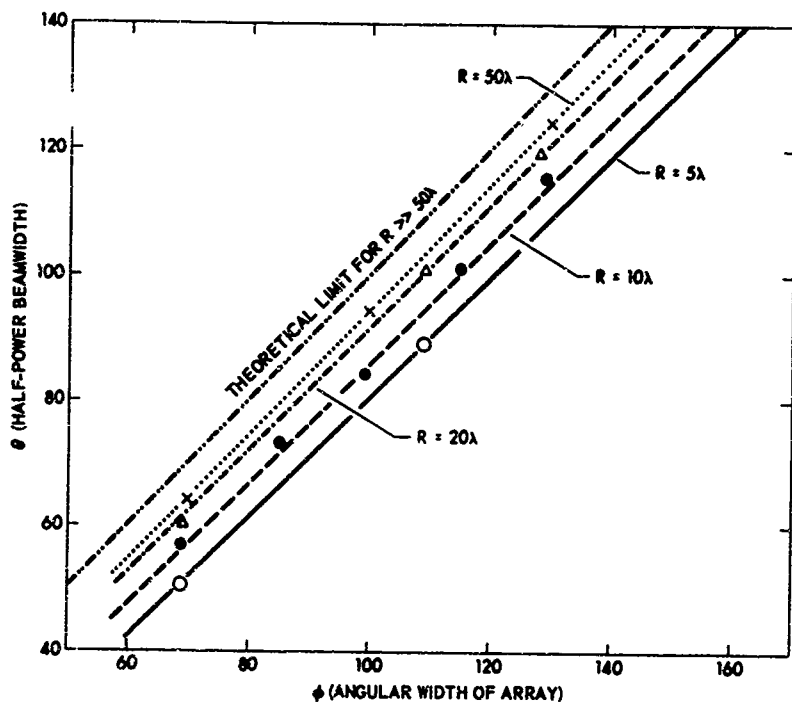
RELATIONSHIP OF ANGULAR WIDTH AND BEAMWIDTH
OF CURVED FACE ARRAYS
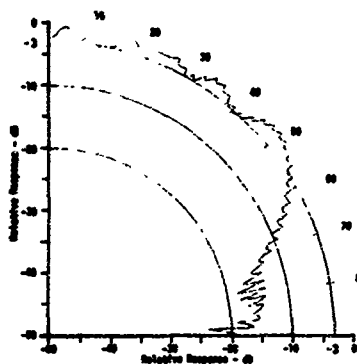
Uniformly Shaded Array
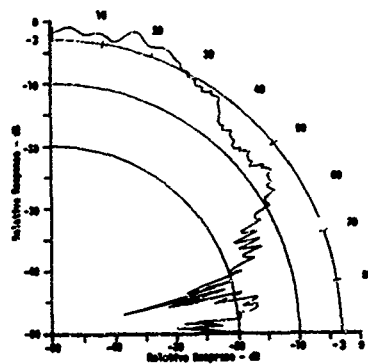
Bizonally Shaded Area
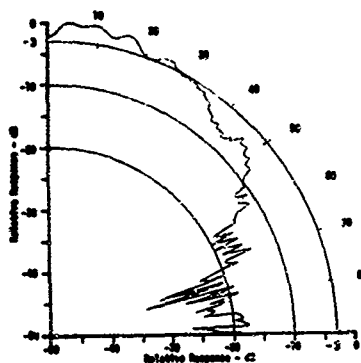
Trizonally Shaded Array
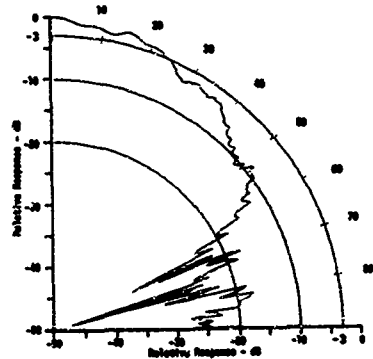
Double Bizonally Shaded Array

EFFECTS OF ZONAL AMPLITUDE SHADING
ON THE BEAM PATTERN OF A CURVED FACE ARRAY

AS-71-1086

In order to determine the influence, if any, of the type of
element used, the same array geometry and amplitude shading were used
to calculate beam patterns using the following individual radiators:

(1) Point

(2) Line

(3) Piston

(4) Circular Ring.

It was noted that for the parameters used (center-to-center spacing
$\approx 0.35\lambda$) the beam patterns do not vary significantly from the patterns
calculated with point sources. However, for larger center-to-center
spacing, the point source approximation is less accurate.

In summary, then, any sector width can be achieved using curved
face arrays. The limitations on the source level are those associated
with the ceramic itself, available power, cavitation limits, and any
limits on the physical size of the array. The amount of ceramic used
to convert electrical to acoustic power can be increased by using a
larger radius of curvature and/or using a longer vertical stave (or
array), with a correspondingly narrower beam.

A wider sector can be covered in both the horizontal and vertical
planes by curving the face of the transducer in both directions.
Beam patterns were calculated for such a configuration, and, as one
might expect, the response in the respective planes was equivalent to
those for the cylindrical configuration with the same radius of
curvature.

B. Directivity Index

In order to relate the beam pattern of a curved face array
configuration to the source levels which can be achieved, the relation-
ship between the beamwidth (or sector covered) and the directivity

59

must be established. The directivity index for any transducer can be calculated from its three-dimensional beam pattern. This involves, however, a numeric or analytic volume integral of the beam pattern. The numeric form is quite time consuming and a general analytic expression for the beam pattern of a curved face array is not readily attainable. Two approximations to the directivity index are outlined below. Results are calculated over a wide range of parameter values.

For wide angle curved face projectors, there are several possible configurations, depending on the nature of the desired pattern and the amount of ceramic needed to handle the required electroacoustical power conversion. The two which will be considered here are the sector of a cylinder (curved in one direction, planar in the perpendicular direction) and the sector of a torus (i.e., two radii of curvature).

C. T. Molloy[29] has derived the directivity index for the first configuration, using the following simplifying assumptions:

1) The intensity of radiation is different from zero only in the region $-\phi/2 \le \theta \le \phi/2$, $-\pi/2 \le \zeta \le \pi/2$.

2) Inside the above defined region, the farfield, the intensity is assumed independent of θ.

3) The dependence of the intensity on γ is assumed to be given by the following expression:

$$I(\theta,\zeta) = \left[\frac{\sin(\pi s \sin(\zeta)/\lambda)}{\pi s \sin(\zeta)/\lambda} \right]^2 \quad ,$$

where the geometry is assumed to be as shown in Dwg. AS-71-1253.

The approximation can be improved by using the actual angular beamwidth instead of the sectoral width (ϕ) as the boundary of the region of insonification.

Field Point

Acoustic Axis
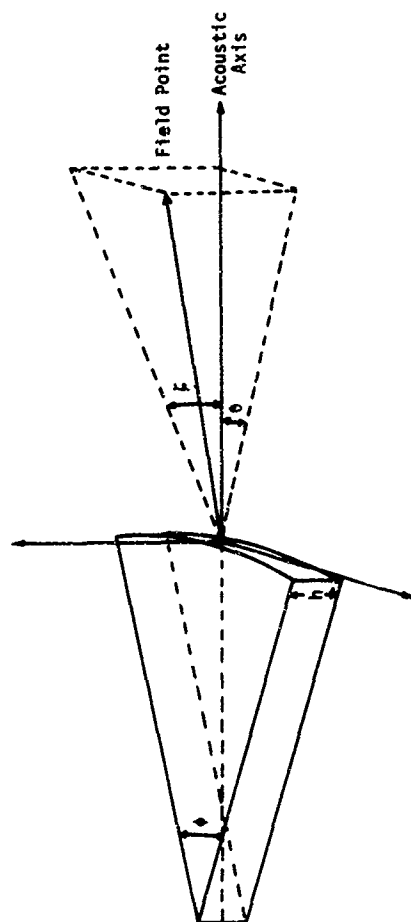
GEOMETRY ASSUMED BY MOLLOY[29]
FOR CALCULATION OF DIRECTIVITY INDEX

AS-71-1253

61

The functional form for directivity index (DI) is given by

$$DI = -10 \log_{10} (W(z) \cdot \alpha) \quad ,$$

where

$$W(z) = \frac{1}{2x} \left[2 \frac{Si(z)}{z} - \frac{\sin^2(z)}{z^2} \right] \quad ,$$

$z = 0.46393 \times$ (vertical height of staves, in inches) $\times$ f
(frequency, in kilohertz),

Si is the integral sine function,

and

α is the angular half-power beamwidth, in radians, in the plane
of curvature of the horn or cylindrical sector.

The values for which the curves were calculated by Molloy were for the
application of loudspeakers in air. The curves have been calculated
for values of general interest in sonar, and are presented in
Dwg. AS-71-1250.

The second configuration projector would be more useful for high
power applications in which a relatively large angular sector is
desired in both the horizontal and vertical planes.

Assume the intensity is uniform and maximum within a solid angle
defined by the angles α and β (as shown in Dwg. AS-71-1251), and is
zero elsewhere.

The directivity ratio (R_p) is defined by Molloy as "... the
ratio of the total acoustic power output of a radiator to the acoustic
power output of a point source producing the same pressure at the same
point on the axis."[29] The directivity index is given by

$$DI = -10 \log_{10} R_p \quad .$$

$$DI = 10 \log_{10} \left(\frac{1}{M(z) \cdot \gamma} \right)$$

where γ is the half-power beamwidth, in radians

z = height of a vertical stave (inches) $\cdot$ frequency (kHz)

Vertical beamwidth = $2 \cdot \arcsin \left(\frac{26.092}{z} \right)$

DIRECTIVITY FUNCTION (MOLLOY[29])

z – kHz-in.

Directivity Function – M(z)

AS-71-1250

63
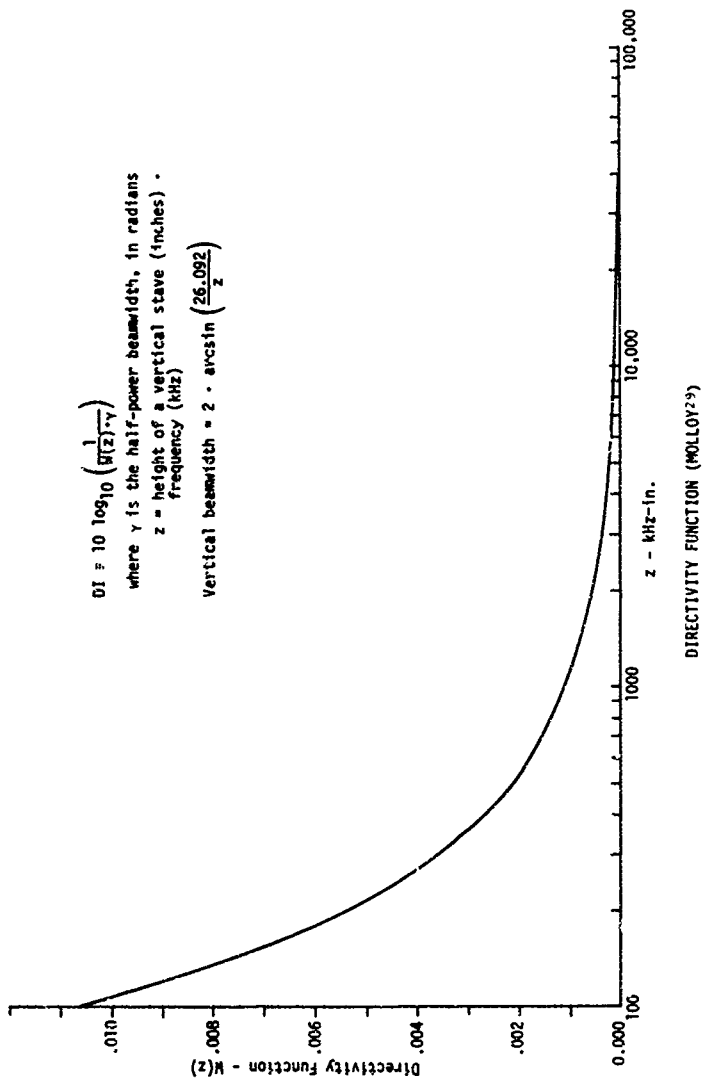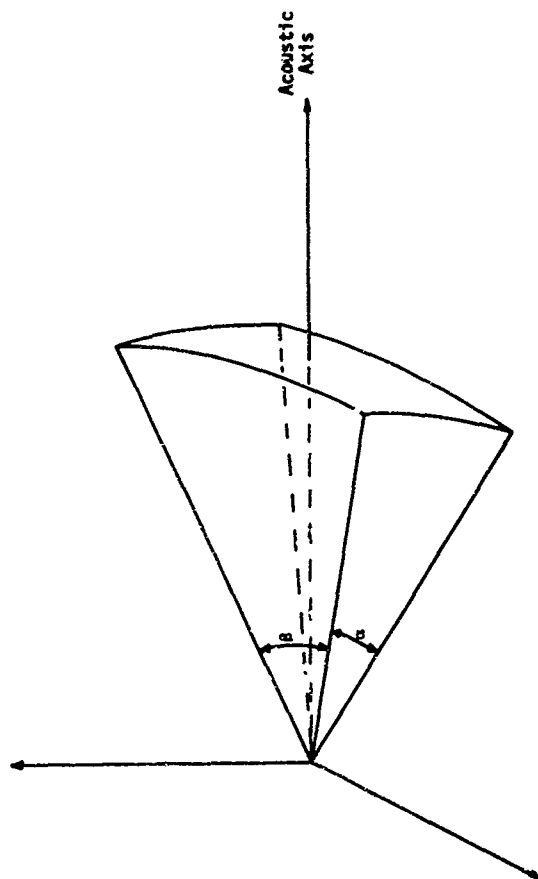
BEAM PATTERN ASSUMED FOR
APPROXIMATION OF DIRECTIVITY INDEX

AS-71-1251

The total acoustic power is the intensity integrated over the entire range of angles α and β, or the volume enclosed by the beam pattern function. The ratio of acoustic power outputs can then be computed from the volume of the directional and omnidirectional patterns. The ratio is

$$R_p = \frac{\text{Volume}_{\text{directional}}}{\text{Volume}_{\text{omnidirectional}}} = \frac{(2\alpha\beta I^3)/\pi}{(4/3)\pi\,I^3} = \frac{\alpha\beta}{2\pi^2}$$

and

$$DI = -10\,\log_{10}\!\left(\frac{\alpha\beta}{2\pi^2}\right) = 10\,\log_{10}\!\left(\frac{2\pi^2}{\alpha\beta}\right) \quad .$$

This formula gives directivity index as a function of the product of the beamwidths in the two perpendicular planes of the acoustic axis of the transducer. The approximation is as good as is the assumption that the volume of the figure shown in Dwg. AS-71-1251 is the volume within the real beam pattern. The "volume" of an actual beam pattern is probably less than the approximation because maximum source level is seldom, if ever, achieved throughout the entire sector.

Directivity index as a function of the product $\alpha\beta$ is shown in Dwg. AS-71-1252. The angles must be in radians for use with this figure.

C. Source Level

The source level of a projector can be calculated from the total acoustic power output and the directivity index:

$$\text{Source Level} = 71.6 + 10\,\log P + DI \ \text{(dB)} \quad ,$$

α and β are as shown in
Dwg. AS-71-1251
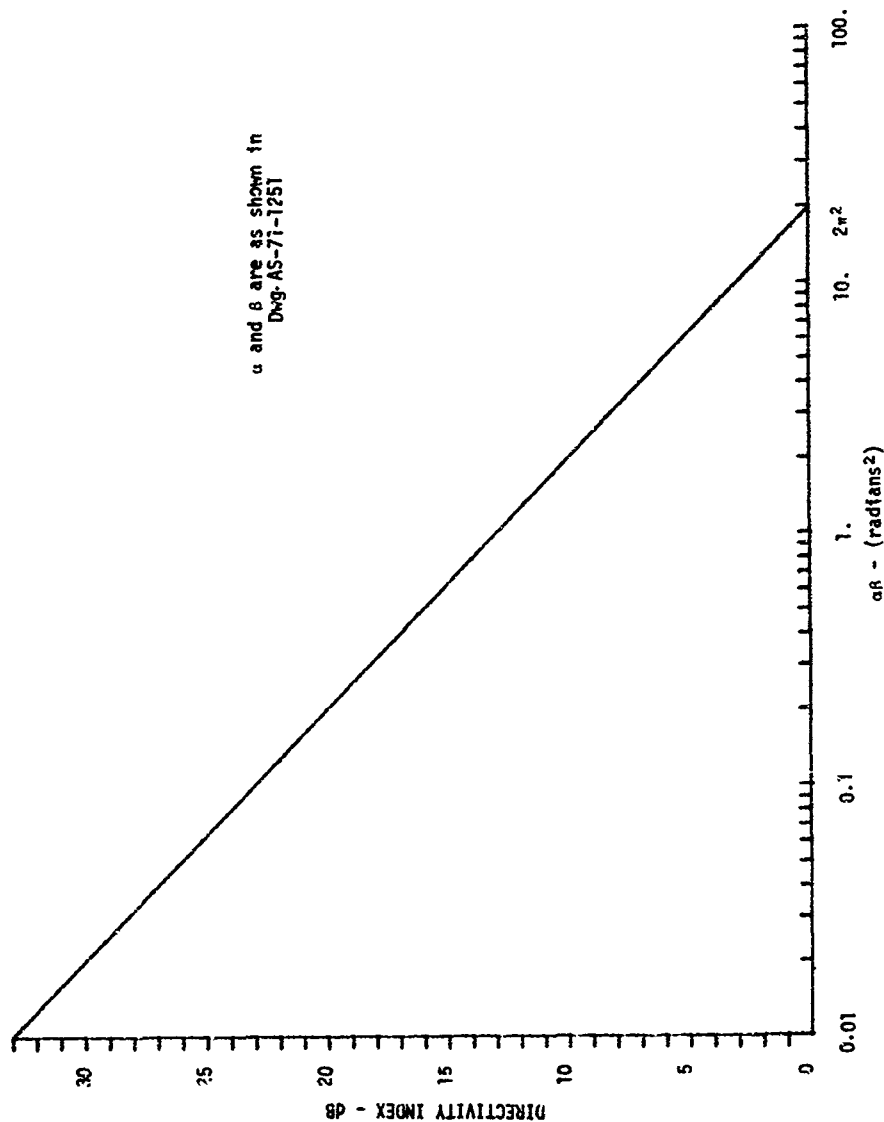
DIRECTIVITY INDEX AS A FUNCTION OF SECTOR COVERAGE

αβ - (radians²)

DIRECTIVITY INDEX - dB

66

AS-71-1252

where

 P = total radiated acoustic power, in watts,

 DI = transmitting directivity index of the transducer, and

71.6 is a factor (in decibels) to convert radiated power in
   watts to intensity, reference the intensity with
   $P=1$ dyne/cm^2.[30]

 Drawing AS-71-1094 shows the relationship between sound pressure level and total acoustic power generated by the transducer, with directivity index as a parameter.

67

DI = Directivity Index
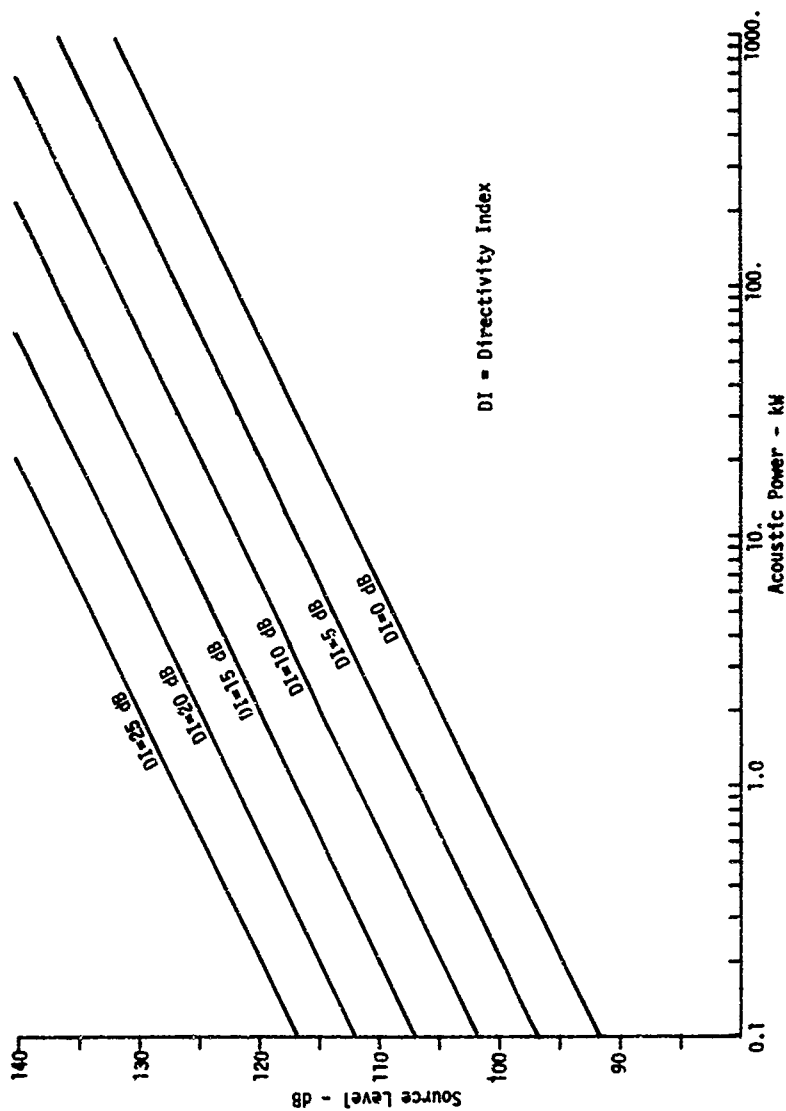
SONAR SOURCE LEVEL AS A FUNCTION OF ACOUSTIC POWER AND DIRECTIVITY INDEX

AS-71-1094

VI. CONCLUSIONS AND RECOMMENDATIONS

A. Summary

The acoustic projection requirements for high power, high search
rate, wide sector sonar systems can be met using curved face trans-
mitter arrays. If additional ceramic is needed to handle the conver-
sion of electrical to acoustic power, a larger radius of curvature can
be used to achieve comparable sector coverage if the arc length is
increased accordingly. This method of designing projectors is acceptable
only as long as the physical size of the transducer remains reasonable
for the specific application.

A direct application of planar array zonal amplitude shading is
not particularly fruitful because the beamwidth is severely narrowed
and because only the highest amplitude elements can be driven at full
power. If the beamwidth of a shaded array is acceptable, more of the
energy is concentrated in the main beam and the array is therefore
more directive.

In order to achieve the sector coverage and source levels at
which this study is aimed (40° to 60° in either direction), signifi-
cantly more electrical power will be required than is used by present
sonars. If, for example, a 30° by 60° beam is to be achieved with a
uniform source level of 120 dB, approximately 10 kW of acoustic output
power is required. Assuming 50% energy conversion efficiency (a typical
value for present systems), 20 kW of electrical power would be required.
State of the art power amplifiers can deliver such levels of power

for duty cycles up to about 0.5%.* A 0.5% duty cycle would provide a system range of 800 yd and range resolution of 25 ft if achieved with a 5 msec pulse and pulse repetition rate of one per second. Better resolution would lead to lower duty cycle and even more readily fulfilled demands for electrical power. Higher repetition rates or cw operation could greatly increase electrical power requirements, but the limitations of the ceramics examined here would be encountered before all available electrical power would be used.

The adverse effects on ceramic performance resulting from high drive levels are documented in Section IV. In summary, calculations predict that:

1) The resonance frequency of thickness mode ceramics shifts to lower frequencies as field level increased.

2) The electroacoustical efficiency drops with increasing field levels.

3) The ceramic temperature increases with increasing field level.

4) The increase in ceramic temperature produces adverse effects such as reduction of resonance frequency and loss of acoustic power output.

The assumptions made in analyzing the problem of electroacoustic energy conversion and associated source levels are necessary as well as instructive in a study such as the one described here. Its results aid in understanding the relevant parameters and serve as guidelines for future work.

---
*Present work at ARL.

70

B. Recommended Future Work

(1) Develop a computer model for transmitting arrays. Such a
model would provide a prediction capability, not only for the failure
of the ceramic, but also for other aspects of array performance
quality. A computer model becomes especially attractive when its
cost is compared to the cost of "trial and error" construction and
testing.

(2) Conduct a theoretical and experimental study of heat transfer
properties of transducer arrays. This study should include the ceramic
backing material, the geometry of the ceramic, the acoustic window,
and the surrounding medium. Whatever energy is not radiated as
acoustic power will be dissipated within the ceramic as generated
heat or given up to mounting losses. In general, a rise in temperature
has two undesirable effects: (a) it adversely affects ceramic per-
formance, and (b) if transmitted to the surrounding medium, it tends
to lower the cavitation threshold. No guidelines are known to exist
on the thermal design of transducers. An initial effort in this area
would in 'ude a literature search for thermal data on the materials used
in various components of transducer systems.

(3) Consider the effects of cavitation on transducer performance.
This item is important because the onset of cavitation is the ultimate
limit of sonar source level. Also, if the cavitation threshold is
exceeded, the load into which the ceramic operates is severely decreased.
Such a decrease causes an increase in electrical power dissipated
within the ceramic, resulting in a rapid and possibly fatal rise in
temperature. A simple model could be developed, using a curve fitted
to published data. Such a model would be of limited scope and would
in no way be a complete formulation of the cavitation process, but
would be useful as a general guideline in a study of sonar performance.

71

The onset of cavitation could most readily be modeled as discrete and complete at a predetermined pressure at the face of the transducer. That pressure would be dependent on frequency, temperature, depth (ambient pressure), and pulselength. This approach ignores many factors such as particulate matter and dissolved gases in the water.

(4) Experimentally verify the model for the transducer array. The credibility and usefulness of any computer model is dependent upon comparison with experimental results. Two sources of experimental data are available: (a) parameters of the acoustic projection phenomenon measured in the laboratory where strict control of conditions can be exercised, and/or (b) published experimental results.

(5) Evaluate the usefulness of newly developed ceramics with a computer model. Two developments reported recently are the whisker-reinforced ceramics[31] and the ferroelectrics containing traces of lanthanum and manganese.[32] The improvement in system performance to be realized by utilizing such materials could be critically examined with a computer model of a projecting array.

REFERENCES

1. H. G. Frey and G. R. Barnard, "Acoustic Detection of Deep Targets in the Ocean" (U), Applied Research Laboratories Technical Report No. 71-5 (ARL-TR-71-5), Applied Research Laboratories, The University of Texas at Austin, Austin, Texas (9 February 1971). SECRET

2. G. R. Barnard, "Minehunting Sonar for MHX; Progress Report" (U), Applied Research Laboratories, The University of Texas at Austin, Austin, Texas (13 July 1970). CONFIDENTIAL

3. R. S. Woollett, "Magnetostrictive Material Requirements for Sonar Transducers - Introduction," JUA(USN) 20 (4), 679-690 (October 1970).

4. J. V. Bouyoucos, "Hydroacoustic Transduction - A Survey," JUA(USN) 11 (3), 327-360 (July 1961).

5. R. S. Woollett, "Theoretical Power Limits of Sonar Transducers," 1962 IRE International Convention Report, PART 6, pp. 90-94.

6. R. J. Urick, Principles of Underwater Sound for Engineers (McGraw-Hill Book Co., Inc., New York, 1967).

7. C. H. Sherman, "Effect of the Near-Field on the Cavitation Limit of Transducers," J. Acoust. Soc. Amer. 35, 1409 (1963).

8. P. L. Smith and A. D. Burbage, "A Comparison of the High-Field-Loss Behavior of Commercial Piezoelectric Ceramics," JUA(USN) 15 (2), 301-305 (April 1965).

9. R. F. Brown, "Environmental Effects on the Properties of Piezoelectric Ceramics," JUA(USN) 15 (2), 284-289 (April 1965).

10. G. E. Martin, "Effects of Static Stress on the Dielectric Elastic and Piezoelectric Properties of Ceramics," JUA(USN) 15 (2), 290-295 (April 1965).

11. D. A. Berlincourt and H. H. A. Krueger, "Behavior of Piezoelectric Ceramics Under Various Environmental and Operating Conditions of Radiating Sonar Transducers," JUA(USN) 15 (2), 266-283 (April 1965).

12. R. Gerson, "Dependence of Mechanical Q and Young's Modulus of Ferroelectric Ceramics on Stress Amplitude," J. Acoust. Soc. Amer. 32 (10), 1297-1301 (October 1960).

REFERENCES (Cont'd)

13. C. P. Germano, "On the Meaning of g and d Constant as Applied to Simple Piezoelectric Modes of Vibration," Clevite Corporation Technical Paper TP-222, Clevite Corporation, Cleveland, Ohio (July 1961).

14. "Status Report Under Contract N00014-70-A-0166" (~), Applied Research Laboratories, The University of Texas at Austin, Austin, Texas (30 June 1971). CONFIDENTIAL

15. "Status Report Under Contract N00014-70-A-0166" (U), Applied Research Laboratories, The University of Texas at Austin, Austin, Texas (25 October 1971). CONFIDENTIAL

16. K. S. Van Dyke, "The Peizo-Electric Resonator and its Equivalent Circuit," Proc. IRE 16, pp. 742-764 (June 1928).

17. W. P. Mason, Electromechanical Transducers and Wave Filters (2nd edition) (D. Van Nostrand Company, Inc., Princeton, New Jersey, 1948), pp. 201-209, 399-404.

18. W. P. Mason, "An Electromechanical Representation of a Piezoelectric Crystal used as a Transducer," Proc. IRE 23 (10), 1252-1263 (October 1935).

19. H. F. Olson, Dynamical Analogies (D. Van Nostrand Company, Inc., New York, 1943), Chapters 8 and 9.

20. H. W. Katz, Solid State Magnetic and Dielectric Devices (John Wiley and Sons, Inc., New York, 1959), Chapters 3 and 5.

21. W. Roth, "Piezoelectric Transducers," Proc. IRE 37, pp. 750-758 (1949).

22. R. N. Thurston, "Effect of Electrical and Mechanical Terminating Resistances on Loss and Bandwidth According to the Conventional Equivalent Circuit of a Piezoelectric Transducer," IRE Trans. on Ultrasonics Engineering UE-7, pp. 16-25 (1960).

23. G. Kossoff, "The Effects of Backing and Matching of the Performance of Piezoelectric Ceramic Transducers," IRE Trans. on Sonics and Ultrasonics SU-13 (1), pp. 20-30 (1966).

24. R. J. Bobber, Underwater Electroacoustic Measurements, Naval Research Laboratory, Underwater Sound Reference Division, Orlando, Florida, July 1970.

25. F. V. Hunt, _Electroacoustics_ (John Wiley and Sons, Inc., New York, 1954).

26. W. P. Mason, _Physical Acoustics and the Properties of Solids_ (D. Van Nostrand Company, Inc., Princeton, New Jersey, 1958) Chapter 3.

27. T. F. Huerter and R. H. Bolt, _Sonics_ (John Wiley and Sons, Inc., New York, 1955), Chapter 4.

28. P. M. Kendig and H. C. Clarke, "Some Effects of Driving a Tonpiltz-type Transducer Element at High Displacement Amplitudes," JUA(USN) $\underline{15}$ (2), 310-313 (April 1965).

29. C. T. Molloy, "Calculation of the Directivity Index for Various Types of Radiators," J. Acoust. Soc. Amer. $\underline{20}$ (4), 387-405 (July 1948).

30. _Introduction to Sonar Technology_, TRACOR, Inc., Document No. 65-211-U(Rev), Austin, Texas (December 1965).

31. W. W. Lester, "The High Drive Properties of a New Composite Ceramic Piezoelectric Transducer Material," Interand Corporation, Rockville, Maryland (28 December 1970).

32. S. Ikegami, U. Ichiro, and N. Takashi, "Electromechanical Properties of $PbTiO_3$ Ceramics Containing La and Mn," J. Acoust. Soc. Amer. $\underline{50}$ (4), 1060-1066 (October 1971).